https://doi.org/10.5194/essd-2026-303
Preprint. Discussion started: 30 June 2026

Open Access Earth System Science Data Discussions

ClimAVA-SWE: A High-Resolution CMIP6-Based Snow Water Equivalent Dataset for the Western United States

Authors

Sajad Khoshnood Motlagh[1*], Kayla Smith[2], Wei Zhang[3], Sarah Null[1], Anna Miller[4], Yoshimitsu Chikamoto[3], Andre Geraldo de Lima Moraes[1]

[1]Utah State University, Department of Watershed Sciences, Logan, UT, USA.

[2]Utah State University, Department of Biology, Logan, UT, USA.

[3]Utah State University, Department of Plant, Soil and Climate, Logan, UT, USA.

[4]Utah State University, Department of Environment & Society, Logan, UT, USA.

[*]Corresponding author: sajad.khoshnoodmotlagh@usu.edu

Abstract

The ClimAVA-SWE dataset provides bias-corrected daily snow water equivalent (SWE) estimates at approximately 4 km spatial resolution across the western United States, publicly available through the Harvard Dataverse and can be accessed via its official repository at https://doi.org/10.7910/DVN/SCD2VT (Khoshnood Motlagh, de Lima Moraes and Smith, 2026). The dataset is generated using the Spatial Interactions Downscaling for Snow Water Equivalent (SPID-SWE) method, a data-driven statistical downscaling framework that integrates high-resolution reference SWE data (NSIDC-0719) with daily outputs from an ensemble of 14 CMIP6 global climate models (GCMs). SPID-SWE employs a dual random forest modeling strategy that explicitly distinguishes snow accumulation and ablation phases, improving seasonal SWE representation relative to single-phase approaches. ClimAVA-SWE spans a historical period (1981–2014) and future projections (2015–2100) under three Shared Socioeconomic Pathways (SSP245, SSP370, and SSP585). The pixel-based design of SPID-SWE independently downscales each grid cell across space and time, preserving both spatial and temporal variability in the SWE signal. Although performance is conditioned on the quality of the driving input data, the dataset demonstrates strong accuracy and computational efficiency, providing a robust and scalable resource for high-resolution climate and hydrological impact applications.

1.Introduction

Snow water equivalent (SWE) is a key metric for quantifying the water content stored in snowpack, integrating snowfall, compaction, and melting processes. As such, it provides a direct link between climate dynamics, hydrology, and water resource management. In many mountainous regions—particularly across the western United States—SWE is the primary contributor to streamflow,

https://doi.org/10.5194/essd-2026-303
Preprint. Discussion started: 30 June 2026

Open Access Earth System Science Data Discussions

sustaining water availability through spring and summer(Mote *et al.*, 2005; Kapnick and Hall, 2012; Li *et al.*, 2017). Over recent decades, numerous observational studies have documented widespread declines in SWE, particularly across the western U.S(Brown and Mote, 2009; Kapnick and Hall, 2012; Klos, Link and Abatzoglou, 2014a; Knowles, 2015; Shi and Wang, 2015; Demaria *et al.*, 2016; Fassnacht *et al.*, 2016; Solander, Bennett and Middleton, 2017; Mote *et al.*, 2018). These observed reductions have increasingly been attributed to anthropogenic climate change(Pierce *et al.*, 2008), raising concerns about future water scarcity, heightened drought risk, and cascading impacts such as increased wildfire activity and ecological stress(L Westerling *et al.*, no date; Mahanama *et al.*, 2012). Climate model projections reinforce these concerns, consistently indicating continued reductions in snowpack, earlier onset of melt, and shifts in runoff timing under future warming scenarios(Brown and Duguay, 2010; Klos, Link and Abatzoglou, 2014b; Solander, Bennett and Middleton, 2017). However, snow responses are not uniform to these changes: some high-latitude and high-elevation regions may experience localized snow increases due to enhanced winter precipitation(Notarnicola, 2020; Kawase *et al.*, 2021). These complex, regionally dependent dynamics highlight the need for accurate, spatially resolved SWE projections to inform water management(Cho and Jacobs, 2020), hazard preparedness, and climate adaptation strategies in vulnerable basins(Callaghan *et al.*, 2011).

Global climate models (GCMs), such as those contributing to the Coupled Model Intercomparison Project Phase 6 (CMIP6), are the primary tools for generating future climate projections(Eyring *et al.*, 2016). GCMs provide essential insights into large-scale climate processes and long-term trends, but their coarse horizontal resolutions (typically 50–300 km) are insufficient for representing the complex terrain and microclimates of mountainous regions(Wood *et al.*, 2004; Maurer *et al.*, 2010; Walton *et al.*, 2017). This deficiency is particularly true for SWE, which is strongly influenced by elevation gradients, aspect, and local precipitation patterns. The direct application of GCM outputs at local scales, therefore, might misrepresent snowpack dynamics and evolution, which are critical for adaptation and planning(Fowler, Blenkinsop and Tebaldi, 2007; Harris *et al.*, 2014; Ekström *et al.*, 2016).

To overcome this limitation, researchers increasingly rely on downscaling techniques(Christensen and Lettenmaier, 2007; Alder and Hostetler, 2019) that translate large-scale GCM outputs into high-resolution climate information, thereby supporting regional and local decision-making(Christensen and Lettenmaier, 2007; Abatzoglou and Brown, 2012; Alder and Hostetler, 2019; Tabari *et al.*, 2021). Downscaling approaches fall into two main categories: dynamical downscaling, which uses regional climate models (RCMs) nested within GCMs to produce physically consistent projections(Eum, Gupta and Dibike, 2020; Keller *et al.*, 2022; Attique, Rientjes and Booij, 2023), and statistical downscaling, which leverages empirical relationships between large-scale predictors and local climate variablesr(Fowler, Blenkinsop and Tebaldi, 2007; Abatzoglou and Brown, 2012; Tabari *et al.*, 2021; Attique, Rientjes and Booij, 2023; Cody Ratterman *et al.*, 2025; Vernon, Zhang and Chikamoto, 2025). While RCMs offer high physical fidelity, their high computational demands

https://doi.org/10.5194/essd-2026-303
Preprint. Discussion started: 30 June 2026

and sensitivity to the prescribed boundary conditions constrain their practicality for large-scale impact assessments(Wood *et al.*, 2004; Ashfaq *et al.*, 2016; Lanzante *et al.*, 2018). Statistical approaches, by contrast, are more computationally efficient and flexible, enabling the generation of large ensembles of high-resolution projections that are particularly valuable for assessing climate impacts(America *et al.*, no date; Payne *et al.*, 2004; Wood *et al.*, 2004; Christensen and Lettenmaier, 2007; Maurer, 2007; Demaria *et al.*, 2016; Alder and Hostetler, 2019). Within statistical downscaling, machine learning (ML) techniques have emerged as powerful tools for capturing complex, nonlinear relationships in climate data. Among the most commonly used ML-based approaches are Artificial Neural Networks (ANNs)(Liu *et al.*, 2010), Support Vector Machines (SVMs)(Chen, Yu and Tang, 2010), and Random Forests (RF) and their extensions, such as the Spatial Interactions Downscaling (SPID) method(de Lima Moraes and Motlagh, 2024). Recent advancements also include deep learning architectures such as Convolutional Neural Networks (CNNs)(Vandal *et al.*, 2017; Baghanam *et al.*, 2024) and hybrid CNN-LSTM models(Zarei *et al.*, 2025). These ML-based methods enhance the flexibility and accuracy of statistical downscaling, enabling more robust high-resolution climate projections for impact.

Despite recent advances, significant gaps remain in the availability of high-resolution snow water equivalent (SWE) datasets across regions. Much of the existing research has relied on coarse-resolution global climate model (GCM) ensembles, single RCM experiments, or limited downscaling efforts applied to a narrow range of models and scenarios(America *et al.*, no date; Plummer *et al.*, 2006; Räisänen, 2008; Brutel-Vuilmet, Ménégoz and Krinner, 2013; Diffenbaugh, Scherer and Ashfaq, 2013; Krasting *et al.*, 2013; Musselman *et al.*, 2017; Matiu and Hanzer, 2022). A variety of SWE products currently exist, yet most are constrained by spatial resolution, temporal coverage, or geographic extent. For example, the Global Snow Monitoring for Climate Research (GlobSnow) provides hemispheric SWE estimates at ~25 km resolution using passive microwave and reanalysis data(Luojus *et al.*, 2021), offering valuable long-term records but limited utility in complex mountainous terrain where coarse pixels smooth steep gradients. Regionally, the Airborne Snow Observatory (ASO) has produced exceptionally detailed 50 m SWE maps derived from LiDAR and modeling for selected mountain basins in California and Colorado(Painter *et al.*, 2016), demonstrating the potential of high-resolution mapping but with limited spatial and temporal coverage. Other gridded datasets, such as Livneh(Livneh *et al.*, no date) and Daymet v4(no date), offer daily SWE estimates at 1–4 km resolution across the contiguous U.S., though their SWE components are derived indirectly from temperature and precipitation rather than explicit snowpack modeling. More recent reanalysis-based products—such as ERA5-Land(Muñoz-Sabater *et al.*, 2021) and MERRA-2(Gelaro *et al.*, 2017) —provide global coverage at 9–25 km resolution but remain too coarse for basin-scale hydrologic and ecological studies. These limitations are particularly pronounced in the western United States, a region where snowpack serves as a critical water resource(Li *et al.*, 2017). Here, many efforts have focused primarily on downscaling temperature and precipitation(Baño-Medina, 2020; Banõ-Medina *et al.*, 2022; Zarei *et al.*, 2025), often overlooking SWE despite its central role in hydrologic systems and climate adaptation

https://doi.org/10.5194/essd-2026-303
Preprint. Discussion started: 30 June 2026

planning. More recently, machine-learning-based studies have begun to explore SWE downscaling(Zakeri, Mariethoz and Girotto, 2024; Damiani *et al.*, 2025; Li *et al.*, 2025), demonstrating the potential of these approaches. However, applications specifically targeting the western United States and future SWE projections remain relatively limited.

Although the growing body of evidence has documented snowpack decline and the associated environmental and societal risks across the western U.S., there remains a pressing need for robust, bias-corrected, high-resolution SWE datasets derived from multi-model GCM ensembles.

To address the above needs, the present study enhances the Spatial Interactions Downscaling (SPID) method to produce a long-term, high-resolution SWE dataset for the region.

Unlike other high-resolution SWE products, SPID-SWE is unique in its computational efficiency and its ability to generate a continuous, bias-corrected SWE dataset spanning a long temporal period (1981–2100) across the entire western U.S. at a fine spatial resolution (~4 km). This combination of spatial and temporal coverage fills a critical gap in existing datasets, enabling both regional and long-term analyses of snowpack dynamics. Using this improved method, we generate a daily SWE dataset derived from 14 global climate models (GCMs) under three future climate scenarios. This long-term future projections establishes a strong foundation for assessing snowpack dynamics with high spatial representation, thereby supporting improved water management, climate risk assessment, and adaptation planning(de Lima Moraes and Motlagh, 2024) in one of North America's most climate-sensitive regions.

2. Methods

2.1. Data Acquisition

ClimAVA-SWE is based on two primary data sources (step 1 in Fig. 1(a)):

Reference SWE Data. We used the University of Arizona's daily snow water equivalent (SWE) dataset (NSIDC-0719, Version 1)(Zeng, Broxton and Dawson, 2018), publicly available through the National Snow and Ice Data Center (https://nsidc.org/data/nsidc-0719/versions/1). This dataset provides daily SWE estimates at a 4-km spatial resolution across the contiguous United States for the period 1982–2023. This resolution is consistent with our previous ClimAVA dataset(de Lima Moraes and Khoshnood Motlagh, 2024a; Khoshnood Motlagh and de Lima Moraes, 2025), allowing for direct comparison and integration across analyses. It is developed by assimilating in-situ measurements from the SNOTEL and COOP networks with gridded meteorological data (precipitation and temperature) from the PRISM dataset(Zeng, Broxton and Dawson, 2018). Owing to its high spatial resolution, long temporal coverage, and integration of multiple data sources, the dataset has been widely adopted in hydrological and climate research(Cho and Jacobs, 2020; Siegel, Fullerton and Jordan, 2022; Roberts-Pierel, Raleigh and Kennedy, 2024).

CMIP6 GCM Data. Daily historical and future projections of snow water equivalent (SWE) from Phase 6 of the Coupled Model Intercomparison Project (CMIP6) were obtained from 14 global

https://doi.org/10.5194/essd-2026-303
Preprint. Discussion started: 30 June 2026

climate models (GCMs) available through the CMIP6 archive(O'Neill *et al.*, 2016), accessed via the Earth System Grid Federation (ESGF) MetaGrid portal (https://aims2.llnl.gov/search). Models were selected based on the following criteria: (1) availability of daily SWE output; (2) inclusion of projections for the SSP245, SSP370, and SSP585 scenarios to ensure coverage across a broad range of socioeconomic and emissions pathways; and (3) a nominal spatial resolution between 50 and 250 km. To ensure consistent sampling across models, only the first realization (r1i1p1f1 or equivalent) of each model was used. These selection criteria resulted in a final ensemble of 14 GCMs (see Table 1).

Table 1. 14 selected CMIP6 Global Climate Models (GCMs). The variant label provides information about realization (r), initialization method (i), physics (p), and forcing (f).

GCM	Variant label	Grid spacing	Institute
EC-Earth3	r1i1p1f1	0.703125° x 0.703125°	European EC-Earth Consortium (Europe)
GFDL-ESM4	r1i1p1f1	1° x 1.25°	Geophysical Fluid Dynamics Laboratory, National Oceanic and Atmosphere Administration (USA)
INM-CM4-8	r1i1p1f1	1.5° x 2°	Institute for Numerical Mathematics (Russia)
INM-CM5-0	r1i1p1f1	1.5° x 2°	Institute for Numerical Mathematics (Russia)
MPI-ESM1-2-HR	r1i1p1f1	0.9375° x 0.9375°	Max Planck Institute for Meteorology (Germany)
ACCESS-ESM1-5	r1i1p1f1	1.24137931° x 1.875°	Commonwealth Scientific and Industrial Research Organization (Australia)
IPSL-CM6A-LR	r1i1p1f1	1.258741259° x 2.5°	Institut Pierre Simon Laplace (IPSL) (France)
MIROC6	r1i1p1f1	1.40625° x 1.40625°	Japan Agency for Marine-Earth Science and Technology (Japan)
AWI-CM-1-1-MR	r1i1p1f1	0.927224° x 0.937°	Alfred Wegener Institute, Helmholtz Centre for Polar and Marine Research (Germany)
BCC-CSM2-MR	r1i1p1f1	1.112091° x 1.125°	Beijing Climate Center, China Meteorological Administration (China)
MIROC-ES2H	r1i1p4f2	1.38903° x 1.40°	Japan Agency for Marine-Earth Science and Technology (Japan)
MPI-ESM1-2-LR	r1i1p1f1	1.849638° x 1.875°	Max Planck Institute for Meteorology (Germany)
MRI-ESM2-0	r1i1p1f1	1.11209° x 1.125°	Meteorological Research Institute, Japan Meteorological Agency (Japan)
UKESM1-0-LL	r1i1p1f2	1.25° x 1.875°	Met Office Hadley Centre / United Kingdom Earth System Model (UK)

2.2. Study Area and data preparation

The western United States—characterized by complex mountainous terrain and diverse climate zones—was selected as the study domain due to its strong dependence on seasonal snowpack (SWE) for water resources, ecological integrity, and socio-economic stability, particularly in support of agriculture, hydropower, and municipal supply(Stewart, Cayan and Dettinger, 2005; Mote *et al.*, 2018; Rahimi *et al.*, 2024). The study area encompasses 11 western U.S. states—Washington, Oregon, California, Idaho, Nevada, Utah, Arizona, Montana, Wyoming, Colorado, and New Mexico.

https://doi.org/10.5194/essd-2026-303
Preprint. Discussion started: 30 June 2026

Prior to analysis, the reference SWE dataset was spatially subset to the 11-state study domain and resampled to match the native grid of each GCM. As detailed in Table 1, 14 GCMs were selected, representing 12 unique native spatial resolutions, ranging from 0.703125° × 0.703125° (EC-Earth3) to 1.849638° × 1.875° (MPI-ESM1-2-LR). The resampling procedure was applied at a daily time step using a pixel-aggregation approach designed to match the spatial footprint of each GCM grid cell. All overlapping 4-km reference pixels within a coarse grid cell were aggregated and averaged, preserving the spatial mean of the original GCM while avoiding interpolation artifacts that can occur during regridding(Rupa Rajulapati *et al.*, no date).

2.3. Bias Correction and Model Training

To reduce systematic biases in the GCM-derived SWE predictors prior to downscaling, a quantile mapping bias correction approach was employed(Li, Sheffield and Wood, 2010; Cannon, Sobie and Murdock, 2015; Enayati *et al.*, 2021; Michel *et al.*, 2024) (see step 3 in Fig. 1(a)). This technique adjusts the statistical distribution of each GCM variable to match that of the resampled reference dataset, thereby aligning the predictors with the reference data and improving the reliability of downscaled SWE estimates. This correction was applied only to pixels and time steps with nonzero SWE values, and all zero SWE observations were excluded when constructing the cumulative distribution functions (CDFs). This exclusion is essential because GCMs contain many more zero-SWE days than reference data, and including these would lead to overestimation of SWE.

https://doi.org/10.5194/essd-2026-303
Preprint. Discussion started: 30 June 2026

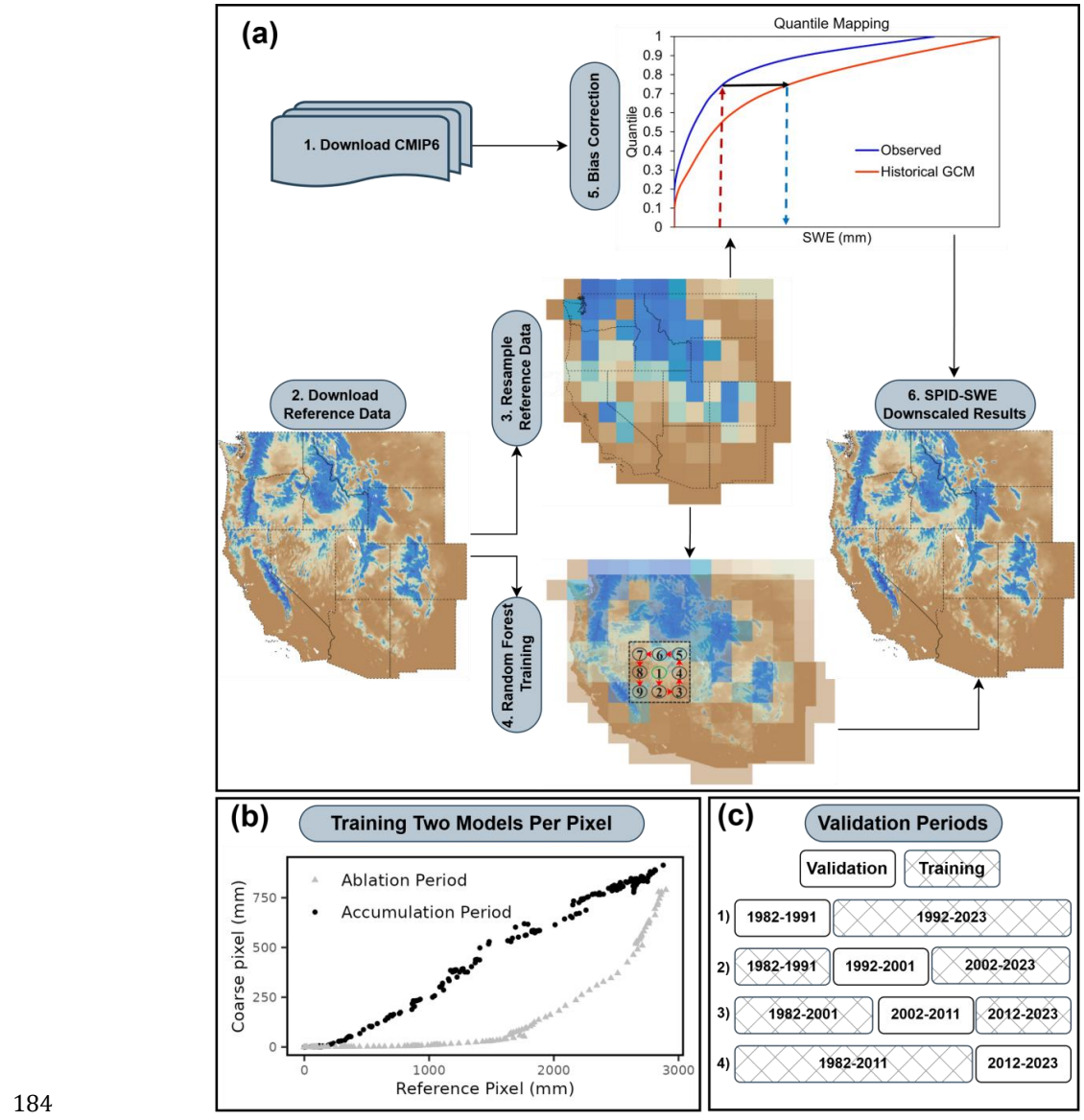

Fig. 1. Overview of the SPID-SWE downscaling framework. (a) Workflow schematic illustrating the five main steps of the approach: (1) acquisition of reference and CMIP6 GCM data, (2) spatial resampling of the reference dataset to match the native resolution of each GCM, (3) bias correction of GCM predictors using quantile mapping (QM), (4) pixel-specific training of random forest models using paired fine-resolution and resampled coarse-resolution reference data, and (5) application of trained models to downscale the bias-corrected GCM data. (b) Rationale for dual-model training per pixel: separate random forest models are developed for the snow accumulation and ablation periods to account for seasonally distinct predictor–predictand relationships. (c) Temporal structure of the validation design, showing the training and downscaling periods used across four non-contiguous time windows spanning 1982–2023.

https://doi.org/10.5194/essd-2026-303
Preprint. Discussion started: 30 June 2026

Following bias correction, downscaling was performed using a modified version of the Spatial Interaction Downscaling (SPID) method (de Lima Moraes and Khoshnood Motlagh, 2024b), referred to here as SPID-SWE. While the original SPID framework relies on a single model per pixel, SPID-SWE introduces a dual-model approach, training separate random forest models for the snow accumulation and ablation periods at each 4-km reference pixel. The separation between accumulation and ablation periods is determined dynamically from the GCM SWE time series by identifying the annual peak SWE (marking the transition to ablation) and the subsequent seasonal minimum (marking the onset of the next accumulation period). This approach allows the method to naturally accommodate shifts in snow season timing, including potential changes under warmer future conditions (Fig. 1(b)).

As shown in Fig. 1(b), the relationship between GCM and reference pixels is approximately linear during the accumulation period, reflecting a relatively direct scaling of coarse-scale predictors to local snowpack growth. In contrast, the ablation period displays a strongly nonlinear, near-exponential pattern. Although it could be hypothesized that linear regression might capture these patterns, in reality, the relationship between coarse-scale predictors and fine-scale SWE varies substantially across pixels. Predictor importance and interactions differ by location, and the central coarse cell is often not the primary driver, with neighboring cells contributing in complex ways. Random Forest models are well suited to handle such nonlinearity and covariable interactions, capturing variable importance and complex predictor relationships that simple linear or exponential models cannot. Linear models might approximate pixels with near-linear accumulation, but they would not generalize across heterogeneous terrain.

Each pixel-specific model is trained using a random forest algorithm(Liaw and Wiener, 2002). The algorithm first identifies the larger (coarse-resolution) GCM grid cell in which it is located. From this central coarse cell, it collects the surrounding eight coarse-resolution cells in a spatial order: down, right, up, up, left, left, down, and down again (see step 4 in Fig. 1(a)). These nine GCM-scale pixels collectively form the predictor set for that fine-resolution pixel. This spatial window captures the local coarse-scale SWE context necessary for accurate downscaling. For pixels near the coastlines or along the national border, the number of available predictor cells may be fewer than nine due to limited spatial coverage in the reference dataset.

2.4. Validation design

To evaluate the robustness and generalizability of the SPID-SWE downscaling framework, we conducted external validation through a series of spatial-temporal validation experiments using the reference resampled SWE dataset spanning 1982 to 2023. Specifically, we downscaled the resampled reference data back to its original resolution and compared the results to the original reference data. Model performance was quantified using standard statistical indicators, including the coefficient of determination (R^2), root mean square error (RMSE), and mean prediction error (MPE). Four distinct training-validation splits were designed to assess model performance across varying climatic regimes and non-contiguous time periods (Fig. 1(c)):

https://doi.org/10.5194/essd-2026-303
Preprint. Discussion started: 30 June 2026

Split 1: Models trained on 1992–2023 and validated in 1982–1991.

Split 2: Models trained on 1982–1991 and 2002–2023 and validated in 1992–2001.

Split 3: Models trained on 1982–2001 and 2012–2023 and validated in 2002–2011.

Split 4: Models trained on 1982–2011 and validated in 2012–2023.

These configurations were designed to test model performance across varying climatic regimes and temporal gaps. For the final application in generating the ClimAVA-SWE dataset, models are trained using the full 42-year reference period (1982–2023) to maximize exposure to diverse climatic conditions and temporal variability.

Two complementary validation approaches were employed: (a) Pixel-Based Validation, applying the statistical indicators above at the daily time scale and at the individual grid-cell level across the western United States; and (b) Watershed-Based Validation, evaluating spatially aggregated SWE metrics over major hydrologic regions within the study domain. Spanning 42 years (1982–2023), this evaluation enables a robust long-term assessment across diverse climatic and topographic settings. To assess how SPID-SWE performs when downscaling from different spatial resolutions, two GCMs representing the extreme spatial resolutions within the CMIP6 ensemble were selected: EC-Earth3 (fine resolution, FR; 0.703125° × 0.703125°) and MPI-ESM1-2-LR (coarse resolution, CR; 1.849638° × 1.875°), which define the resolution bounds of the selected GCMs and allow evaluation of SPID-SWE performance across scales.

2.5. SPID-SWE Computational Demand

The SPID-SWE method is designed to be computationally efficient and scalable, making it accessible even for users with limited high-performance computing (HPC) resources. All computations in this study were performed on AMD 7713P nodes equipped with 64 cores and 256 GB of memory. The 4-km reference SWE dataset covers the western U.S., totaling 188,786 pixels. Since SPID-SWE trains two random forest models per pixel (for snow accumulation and ablation periods), 377,572 models were trained per GCM. Across the 14 GCMs used in this study (see Table 1), this amounts to more than 5.28 million models.

To optimize the efficiency of model training, we divided two nodes into six concurrent jobs, each using 20 cores and 80 GB of RAM. This setup achieved a training rate of approximately 2,700 pixels per minute per job. As a result, the entire training process for all 14 GCMs was completed in ~5.5 hours.

Once the models were trained, the downscaling phase was performed using four parallel jobs, each using 32 cores and 120 GB of memory. Each downscaling job processed 20 NetCDF files per model: two for the historical period and six for each of the three SSP scenarios (SSP245, SSP370, SSP585). Each file, representing approximately 15 years of daily data, required around 2.5 hours to downscale. This results in: ~50 hours of processing per GCM (20 files × 2.5 hours) and ~700 total

https://doi.org/10.5194/essd-2026-303
Preprint. Discussion started: 30 June 2026


Open Access Earth System Science Data Discussions

hours for all 14 GCMs, equivalent to ~29 days of runtime sequentially. However, with four concurrent jobs, the actual total runtime was reduced to approximately 7.3 days.

3.Validation and Uncertainty Assessment

Results from both pixel-based and watershed-based validation approaches are presented below, spanning 42 years (1982–2023) across diverse climatic and topographic settings of the western United States.

3.1. Grid-cell Level Validation

Validation results for the two bounding spatial resolutions—FR (0.703125° × 0.703125°; EC-Earth3) and CR (1.875° × 2.5°; MPI-ESM1-2-LR)—are shown in Fig 2. Using results derived from both FR and CR inputs, SPID-SWE demonstrates strong performance in areas with high snow accumulation, such as the Sierra Nevada, Cascade Range, and Rocky Mountains. These mountainous regions correspond to higher R^2 values, shown in blue on the maps, indicating a close match with reference SWE data. In contrast, flatter, low-SWE areas like California's Central Valley and southern portions of Arizona and Nevada exhibit lower R^2 values (yellow to red tones).

Accuracy increases systematically with peak SWE magnitude. For the highest SWE category (300–3024 mm), R^2 values approached 1.0 for both FR and CR. Although absolute RMSE values tend to be larger in regions with greater SWE due to higher magnitudes, expressing RMSE as a percentage of observed SWE reveals that relative errors remain small. This indicates that the method maintains strong proportional accuracy, particularly in areas with substantial snowpack. The mean prediction error (MPE) follows a similar pattern, remaining close to zero across all SWE classes and indicating no systematic bias. Overall, when averaged across the entire domain, FR inputs outperform CR, with mean R^2 values of 0.68 versus 0.64, RMSE values of 11.9 mm versus 12.7 mm, and lower MPE values (0.02 mm versus –0.016 mm), demonstrating the benefits of finer input resolution for capturing spatial variability in SWE. Higher performance in mountainous regions should not be interpreted as the model explicitly resolving fine-scale terrain variability; rather, these regions typically exhibit stronger and more persistent SWE signals, which improve the statistical predictability of SWE.

https://doi.org/10.5194/essd-2026-303
Preprint. Discussion started: 30 June 2026

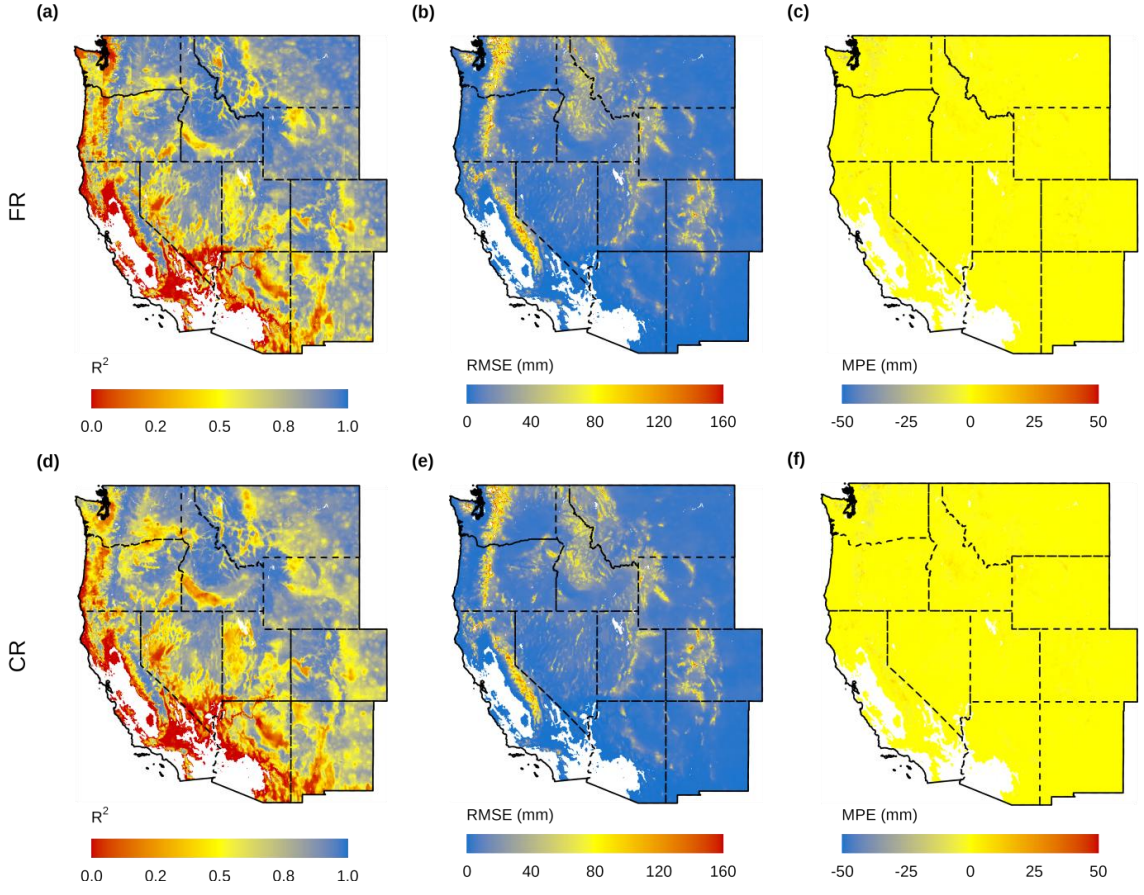

Fig. 2. Validation of daily snow water equivalent (SWE) downscaling from the finest (FR) and coarsest (CR) spatial resolutions. Panels (a)–(c) show the spatial distribution of the coefficient of determination (R^2), root mean square error (RMSE), and mean prediction error (MPE) for FR across the western United States. Panels (d)–(f) show the same metrics for CR.

To further evaluate spatial fidelity and climatological realism, we turn to the long-term mean peak SWE patterns shown in Fig. 3. Evaluation of the 42-year mean annual peak SWE highlights the ability of SPID-SWE to preserve climate realism and spatial consistency in the downscaled data. The reference dataset (Fig. 3(a)) shows strong spatial gradients and orographic patterns, with high SWE values concentrated in mountainous regions such as the Sierra Nevada, Cascades, and the Central and Northern Rockies, consistent with expected climatological spatial distributions. Comparisons with the FR (Fig. 3(b)) and CR (Fig. 3(c)) downscaled products reveal small mean biases of –1.54 mm and –4.20 mm, respectively, indicating strong agreement in domain-wide SWE magnitudes. However, localized discrepancies emerge in high-elevation zones—particularly in the Rockies,

https://doi.org/10.5194/essd-2026-303
Preprint. Discussion started: 30 June 2026

Wasatch, and Sierra Nevada—where SWE amounts are highest. These differences, while visually distinct, remain relatively small in proportion to the total SWE (often >1000 mm), further supporting that the SPID-SWE method performs well in preserving spatial accuracy, particularly in snow-dominated regions.

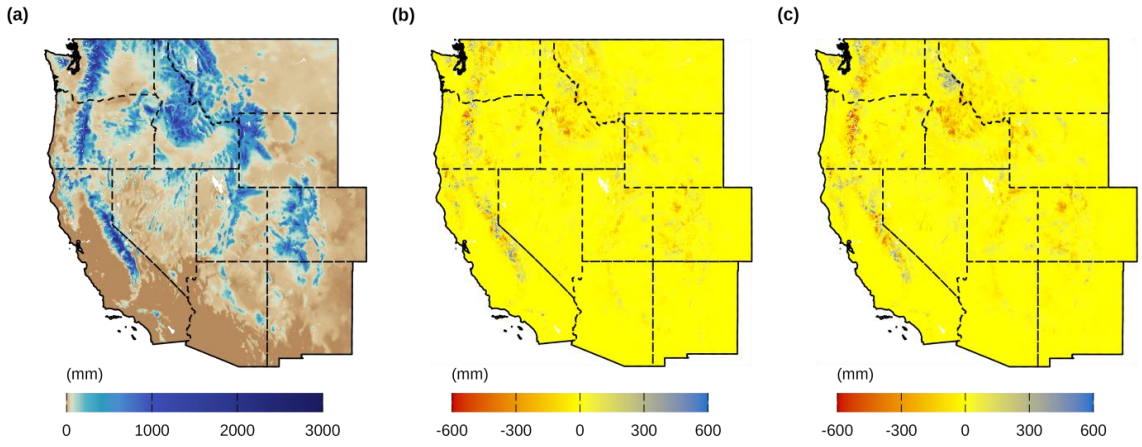

Fig. 3. Forty two-year annual average peak snow water equivalent (SWE) from the reference data shown in panel (a) and their difference to SPID-SWE downscaled data from finest (FR) resolution in panel (b) and coarsest (CR) spatial resolution in panel (c).

3.2. Watershed-Based Validation

Four representative hydrologic basins in the western U.S. were selected: the Upper Colorado River Basin, Great Salt Lake Basin, Sacramento–San Joaquin Basin, and Willamette Basin. These basins encompass a broad range of climatic, topographic, and hydrologic conditions—from arid, high-elevation snow-dominated regions to temperate, mixed-rain–snow systems—making them representative of the diverse snow regimes across the western United States. Model performance is evaluated using three statistical metrics (R^2, RMSE, and MPE) applied to (i) daily snow water equivalent (SWE) time series and (ii) annual maximum SWE, enabling quantitative comparison of downscaled products against the reference dataset.

Overall, the SPID-SWE outputs demonstrate excellent agreement with the reference dataset across all basins and throughout the 42-year evaluation period, as evidenced by high R^2 (≥ 0.96) and low errors for both daily SWE and annual maximum SWE (Table 2). At the daily time-step, both FR and CR reproduce the seasonal evolution and interannual variability of SWE with very high fidelity across all basins ($R^2 \approx 0.99$). However, FR consistently yields lower RMSE than CR, indicating improved representation of SWE magnitude. This improvement is most pronounced in the Great Salt Lake and Willamette basins, where daily RMSE is reduced by approximately 33% and 55% relative to CR, respectively. MPE remains small for both approaches, with FR generally exhibiting slightly lower bias across basins.

https://doi.org/10.5194/essd-2026-303
Preprint. Discussion started: 30 June 2026

For annual maximum SWE, both FR and CR capture interannual variability well (R^2 = 0.94–0.98), including years with extreme snow accumulation. Nevertheless, FR systematically improves peak SWE magnitude relative to CR across all basins, as reflected by lower RMSE values. In the Upper Colorado River Basin, FR reduces annual maximum SWE RMSE from 4.79 mm to 2.94 mm, while in the Great Salt Lake Basin RMSE decreases from 12.15 mm to 9.19 mm. Similar improvements are observed in the Sacramento–San Joaquin Basin, where FR lowers RMSE by approximately 25% relative to CR. The Willamette Basin exhibits the weakest overall agreement among the four basins, with CR showing substantially higher errors (RMSE = 21.00 mm, R^2 = 0.88) for annual maximum SWE. Even in this basin, FR provides a notable improvement, reducing RMSE by nearly 50% and increasing R^2 to 0.96. Across all basins and both temporal scales, FR downscaling yields more accurate SWE magnitudes than CR, particularly during years with high snow accumulation. These results demonstrate that while both approaches preserve large-scale SWE variability, fine-resolution inputs more effectively constrain SWE magnitude, especially for annual maxima and in topographically complex or snow-dominated basins.

Table 2. Basin-aggregated performance metrics for daily and annual maximum snow water equivalent (SWE) derived from resampled downscaled model outputs used for SPID-SWE validation, compared against the reference dataset.

Basin	Model	Type	R^2	RMSE	MPE
Upper Colorado	FR	Annual Max SWE	0.98	2.94	1.04
Upper Colorado	CR	Annual Max SWE	0.96	4.79	0.10
Great Salt Lake	FR	Annual Max SWE	0.96	9.19	0.09
Great Salt Lake	CR	Annual Max SWE	0.94	12.15	-1.25
Sacramento -San Joaquin	FR	Annual Max SWE	0.98	6.70	1.49
Sacramento -San Joaquin	CR	Annual Max SWE	0.97	8.92	1.023
Willamette	FR	Annual Max SWE	0.96	10.80	2.26
Willamette	CR	Annual Max SWE	0.88	21.00	-0.03
Upper Colorado	FR	Daily SWE	0.99	1.19	0.10
Upper Colorado	CR	Daily SWE	0.99	1.78	0.01
Great Salt Lake	FR	Daily SWE	0.99	2.80	0.14
Great Salt Lake	CR	Daily SWE	0.99	4.18	0.04
Sacramento -San Joaquin	FR	Daily SWE	0.99	2.21	0.11
Sacramento -San Joaquin	CR	Daily SWE	0.99	3.21	0.14
Willamette	FR	Daily SWE	0.99	4.40	0.13
Willamette	CR	Daily SWE	0.96	9.79	-0.26

https://doi.org/10.5194/essd-2026-303
Preprint. Discussion started: 30 June 2026

353

354 To provide an evaluation of SPID-SWE against independent point-scale observations and to
355 illustrate model behavior beyond domain-wide statistical metrics, annual peak SWE from the Split
356 1 validation downscaled output (models trained on 1992–2023, applied to 1982–1991 using EC-
357 Earth3) was compared against SNOTEL station measurements at four sites: Echo Peak, CA (Sierra
358 Nevada); Somsen Ranch, ID (Bear River Range); Island Park, ID (Snake River Plain); and Joe Wright,
359 CO (Rocky Mountains) (NRCS, 2026) (Fig. 4). These SNOTEL observations were not used in the
360 training of SPID-SWE or in the construction of NSIDC-0719, making this a fully independent
361 evaluation. It is important to note that the downscaled output used here is the Split 1 validation
362 product — derived from models trained exclusively on 1992–2023 data and applied backwards to
363 1982–1991 — rather than the final ClimAVA-SWE dataset, which uses the full 42-year training
364 period. As shown in Fig. 4, the validation downscaled output and SNOTEL observations track
365 interannual variability in peak SWE consistently across all four stations and throughout the 10-year
366 evaluation period, capturing both wet years (e.g., 1983, 1984) and dry years (e.g., 1987, 1988) with
367 reasonable fidelity. The reference dataset (NSIDC-0719) shows strong agreement with SNOTEL
368 across all sites (R^2 = 0.93–0.98), confirming its reliability as a gridded training target. R^2 values
369 between SNOTEL and the validation downscaled output are 0.85, 0.94, 0.92, and 0.80 for Echo Peak,
370 Somsen Ranch, Island Park, and Joe Wright, respectively, indicating strong to very strong agreement
371 across all stations with a mean R^2 of 0.88. Overall, these results demonstrate that SPID-SWE
372 produces physically plausible SWE estimates that are consistent with independent observations
373 across diverse hydroclimatic and topographic settings, providing confidence in the dataset beyond
374 what statistical validation metrics alone can convey.

https://doi.org/10.5194/essd-2026-303
Preprint. Discussion started: 30 June 2026

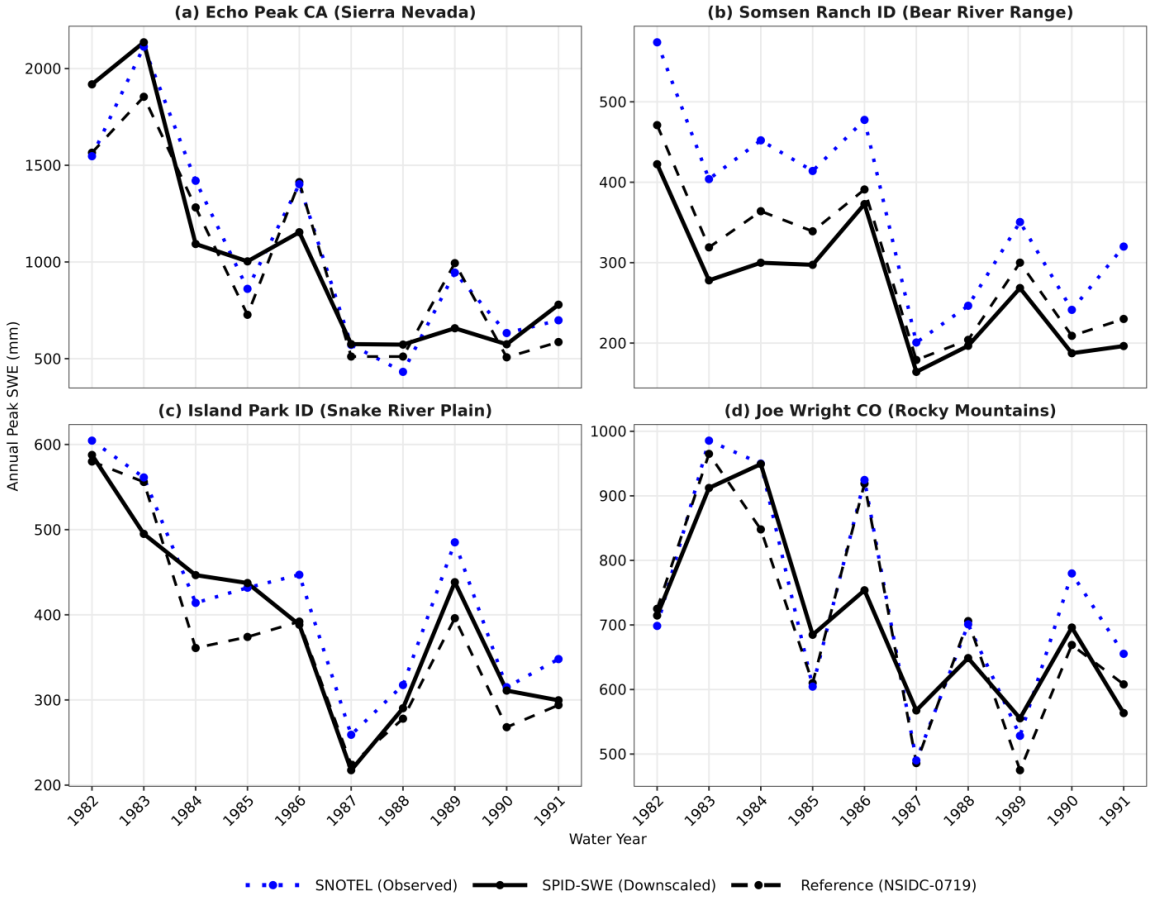

Fig. 4. Comparison of annual peak snow water equivalent (SWE) at four SNOTEL stations across the western United States for the independent validation period 1982–1991: (a) Echo Peak, CA (Sierra Nevada); (b) Somsen Ranch, ID (Bear River Range); (c) Island Park, ID (Snake River Plain); and (d) Joe Wright, CO (Rocky Mountains). Blue dotted lines represent SNOTEL point observations, which are independent of both the training and reference datasets. black solid lines represent SPID-SWE validation downscaled output from Split 1 (models trained on 1992–2023, applied to 1982–1991 using EC-Earth3 as the driving input). Black dashed lines represent the gridded reference dataset (NSIDC-0719).

3.3. Evaluation of GCM SWE and Bias Correction Effects

The performance of 14 CMIP6 GCMs in simulating key snow water equivalent (SWE) metrics across the western United States, evaluated both before bias correction (BC) and after bias correction (AC) is presented in Table 3. The primary objective is to assess whether bias correction improves model fidelity with respect to reference data SWE characteristics and seasonal dynamics.

https://doi.org/10.5194/essd-2026-303
Preprint. Discussion started: 30 June 2026

The evaluation includes a comprehensive set of metrics grouped into three categories that capture essential aspects of snowpack behavior. The following sections provide concise definitions for each metric used in this analysis.

1. Magnitude Metrics:
   a. Peak SWE Value: The maximum snow water equivalent (SWE) recorded within a given water year.
   b. Mean Seasonal SWE: The average SWE over the defined snow season (typically from the onset of persistent snow to melt-out).
2. Timing Metrics:
   a. Snow Onset Day: The first day of the water year on which SWE exceeds a minimum threshold (e.g., 1 mm) and remains above that threshold for a sustained period, indicating the start of seasonal snow accumulation.
   b. Peak SWE Timing: The day of the water year on which Peak SWE occurs.
   c. Melt-Out Day: The last day of the water year on which SWE falls to zero (or below a minimal threshold), marking the complete disappearance of the seasonal snowpack.
   d. Snow Duration: The total number of days between Snow Onset Day and Melt-Out Day.
3. Spatial and Trend-Based Metrics:
   a. Snow-Free Days: The number of days in the water year during which SWE remains at zero, representing the absence of snow cover.
   b. Sen's Slope (Peak SWE): A non-parametric estimate of the long-term trend in Peak SWE values over the analysis period, calculated as the median of pairwise slopes between annual observations(Pranab Kumar Sen, 1968).
   c. Sen's Slope (Seasonal SWE): A comparable trend estimate computed for Mean Seasonal SWE.

Metrics were computed at the grid-cell level over regions with snow, excluding snow-free areas. For each grid cell, the full time series of daily SWE was used to calculate each metric. After computing metrics at each grid cell, spatial averages over the snow-covered area were calculated to summarize results at the regional scale. No weighting based on snow amount was applied. This approach ensures that the metrics reflect the spatial variability of snow across the snow-covered landscape while excluding regions without snow. For each model, metric values are reported as the difference between the GCM output and the reference data (i.e., GCM − Reference). Negative values indicate underestimation, while positive values reflect overestimation. Improvements are identified when AC (After Bias Correction) values move closer to zero or show reduced absolute bias compared to BC (Before Bias Correction).

3.3.1. GCM Outputs Evaluation

Raw GCM outputs (prior to bias correction) generally underestimated peak SWE across the western U.S. relative to the reference dataset, with an ensemble mean bias of −42.4 mm. EC-Earth3 and IPSL-CM6A-LR slightly overestimated peak values, whereas several others (e.g., INM-CM5-0(-83.6 mm),

https://doi.org/10.5194/essd-2026-303
Preprint. Discussion started: 30 June 2026

ACCESS-ESM1-5(-64.5 mm), UKESM1-0-LL(-97.3 mm)) underestimated by more than 60 mm. Mean seasonal SWE followed a similar pattern, with the ensemble consistently underestimating values (−32.5 mm on average). The largest negative biases occurred in ACCESS-ESM1-5(−52.4 mm), INM-CM5-0 (−51.8 mm), and INM-CM4-8 (−50.8 mm), whereas EC-Earth3 slightly overestimated seasonal SWE by 17.5 mm.

GCMs produced pronounced biases in snow duration, simulating an average of 97 fewer snow-covered days than reference data. Several models (e.g., INM-CM4-8, MPI-ESM1-2-HR, ACCESS-ESM1-5, INM-CM5-0) underestimated coverage duration by more than 120 days. Snow onset occurred later than the reference, with an average delay of +11 days, and in some cases (e.g., INM-CM4-8 and INM-CM5-0) by more than three weeks. Models generally reached peak SWE too early, with an ensemble mean bias of −21.8 days. However, EC-Earth3 peaked 4 days later and UKESM1-0-LL about 68 days later than observed. All models simulated melt-out too early, 18 to 91 days ahead of the reference, resulting in a large overestimation of snow-free days (+108 on average). In contrast, SWE trends (Sen's slope) in GCMs are similar to those in the reference data, with biases in peak slope being small for most models, and the ensemble mean near zero. Only minor departures were observed for the seasonal slope as well (~+0.2).

Discussions
Earth System Science Data
Open Access

Table 3. Performance evaluation of SWE metrics before and after bias correction across 14 CMIP6 GCMs

	Peak SWE Value		Mean Seasonal SWE		Snow Duration		Snow Onset Day		Peak SWE Timing		Melt Out Day		Snow Free Days		Peak Slope		Seasonal slope	
	BC	AC	BC	AC	BC	AC	BC	AC	BC	AC	BC	AC	BC	AC	BC	AC	BC	AC
EC-Earth3	29.3	-2.6	17.5	-7.2	-24.5	-27.4	-7.8	-3.7	3.9	3.9	-18	-18	34.7	34.7	-0.1	0.3	0.2	0.3
GFDL-ESM4	-14.3	22.9	-31.8	-17.7	-87.8	-73.1	3.6	-5.5	-27.3	-27.3	-51	-36	108.4	108.4	0.5	0.5	0.4	0.4
INM-CM4-8	-53.9	18.0	-50.8	-27.8	-127	-87.1	29.3	2.7	-31.1	-31.1	-89	-59	123.6	123.6	0.4	0.4	0.4	0.2
INM-CM5-0	-83.6	-25.0	-51.8	-29.4	-126	-89.3	25.2	2.4	-34.0	-34.0	-91	-64	126.5	126.5	0.0	-0.1	0.2	-0.1
MPI-ESM1-2-HR	-46.2	5.8	-43.9	-31.4	-126	-110	13.1	0.2	-40.7	-40.7	-74	-49	162.3	162.3	0.5	0.6	0.4	0.5
ACCESS-ESM1-5	-64.5	17.8	-52.4	-30.3	-139	-97.7	23.6	-3.2	-40.8	-40.8	-89	-45	136.7	136.7	-0.1	-0.5	0.1	-0.1
IPSL-CM6A-LR	3.4	5.5	-16.0	-15.1	-72.5	-55.4	-4.2	-9.1	-25.9	-25.9	-31	-16	76.9	76.9	1.0	0.9	0.7	0.7
MIROC6	-43.9	-27.3	-33.6	-23.4	-89.8	-85.0	18.0	16.3	-24.8	-24.8	-66	-63	126.1	126.1	-0.2	-0.4	0.1	0.0
AWI-CM-1-1-MR	-52.2	4.7	-43.0	-18.9	-124	-68.4	11.5	-18.1	-41.4	-41.4	-72	-17	98.3	98.3	-0.3	-0.2	0.2	0.0
BCC-CSM2-MR	-59.9	-27.2	-24.7	-16.2	-83.4	-57.6	-0.7	-15.2	-25.0	-25.0	-46	-15	83.7	83.7	0.4	0.4	0.3	0.2
MIROC-ES2H	-68.9	-44.9	-26.0	-19.5	-74.1	-72.7	14.1	14.5	-20.3	-20.3	-59	-57	107.6	107.6	-0.8	-0.7	-0.3	-0.3
MPI-ESM1-2-LR	-51.3	2.2	-45.7	-32.1	-134	-115	16.0	2.0	-42.4	-42.4	-85	-59	165.5	165.5	0.5	0.5	0.4	0.3
MRI-ESM2-0	9.5	25.7	-20.8	-18.2	-79.1	-63.7	5.3	-0.2	-22.8	-22.8	-47	-36	94.6	94.6	-0.2	-0.2	0.1	0.1
UKESM1-0-LL	-97.3	-95.8	-31.9	-14.4	-69.9	-50.9	8.6	-10.6	68.1	68.1	-41	0.4	71.3	71.3	-1.1	-1.7	-0.4	-1.0
Average	-42.4	-8.6	-32.5	-21.5	-97.1	-75.3	11.1	-2.0	-21.8	-21.8	-61	-38	108.3	108.3	0.0	0.0	0.2	0.1

https://doi.org/10.5194/essd-2026-303
Preprint. Discussion started: 30 June 2026

https://doi.org/10.5194/essd-2026-303
Preprint. Discussion started: 30 June 2026

3.3.2. Bias Correction Evaluation

Bias correction substantially improved the alignment of GCM-simulated SWE magnitude metrics with the reference dataset across most models, although the degree of improvement varied by model. Ensemble-mean biases in annual peak SWE and mean seasonal SWE were reduced from −42.4 mm and −32.5 mm before correction to −8.6 mm and −21.5 mm after correction, respectively, indicating a significant reduction in underestimation. Mean seasonal SWE improved for all models, with an average improvement of ~34% across the 14 models, while peak SWE improved for nearly all models, averaging ~80%. Several models showed marked improvements, such as MPI-ESM1-2-HR (−46.2 mm to 5.8 mm), AWI-CM-1-1-MR (−52.2 mm to 4.7 mm), and MPI-ESM1-2-LR (−51.3 mm to 2.2 mm). Excluding MRI-ESM2-0 and UKESM1-0-LL, which showed no improvement or slight worsening, the correction was highly effective. UKESM1-0-LL remained strongly biased in peak SWE values after correction (−97.3 mm to −95.8 mm). This bias stems from unrealistic zero SWE values throughout the years 2010, 2011, and 2014, which prevented meaningful correction (Fig. 5). This limitation arises because the bias correction method used does not adjust zero outputs from GCMs (as noted in (Jörg-Hess *et al.*, 2014; Michel *et al.*, 2024)); As a result, days with simulated zero SWE remain unchanged after correction. While excluding zeros from the CDF construction allowed bias correction to function for most of the UKESM1-0-LL historical output, our approach cannot generate SWE where none exists, and this model was excluded from the ensemble due to unrealistic zero-SWE predictions. Overall, ensemble-mean peak SWE biases improved by ~90% (Table 1), and after applying bias correction, simulated SWE curves aligned more closely with the reference data, demonstrating clear improvement in model performance.

Analysis of different SWE metrics further highlighted systematic biases in raw GCMs, consistent with findings from previous studies (e.g., (Maloney *et al.*, no date; Mccrary and Mearns, no date; Mearns *et al.*, 2012)). Change in snow duration through time was consistently negative, indicating fewer days with snow on the ground than in the reference(Callaghan *et al.*, 2011; Derksen *et al.*, 2012; Trujillo and Molotch, 2014). Across all models, GCM outputs contained substantially more zero-SWE days compared to the reference dataset, in line with observations that GCMs often simulate more snow-free days(Mccrary and Mearns, no date). On average, GCMs produced roughly twice as many zero-SWE days as the reference, with a mean ratio of about 2.08. Model-specific ratios ranged from ~1.54 for EC-Earth3 to ~2.81 for INM-CM5-0. Notably, over half of the models exceeded a ratio of 2.0, underscoring GCMs often overpredict snow-free conditions relative to the reference dataset.

Timing metrics showed mixed results. Snow duration improved slightly, with the ensemble mean bias reduced from −97.1 days before correction to −75.3 days after. Several models, including AWI-CM-1-1-MR, INM-CM4-8, and INM-CM5-0, reduced their biases by over 30 days. Snow onset day also showed some improvement, with the average delay reduced from +11.1 days to −2.0 days, indicating that models simulated onset closer to the reference timing. INM-CM4-8, for example, improved from a delay of 29.3 days to just 2.7 days. Melt-out day biases were similarly reduced,

https://doi.org/10.5194/essd-2026-303
Preprint. Discussion started: 30 June 2026

with the ensemble mean improving from −61 days to −38 days. Most models showed earlier melt-out in the raw outputs, and bias correction shifted these values closer to the reference, though EC-Earth3 remained unchanged at −18 days.

In contrast, no change was identified for Peak SWE timing or Snow-Free Days across any of the models. The ensemble mean bias for peak timing remained at −21.8 days, and snow-free days stayed at +108.3 days. This outcome is expected because the bias correction method adjusts the statistical distribution of daily SWE values but does not alter zero values. Consequently, metrics related to timing or binary snow presence/absence remain insensitive to this correction approach. Overall, the results demonstrate that bias correction effectively improves peak SWE estimates and, to a lesser extent, mean seasonal SWE, providing greater confidence in interpreting snowpack magnitudes and spatial patterns. However, timing-related dynamics, particularly the number of snow-free days and the seasonal progression of snow accumulation and melt, remain strongly biased, reflecting structural limitations of the GCMs themselves.

The application of Quantile Mapping (QM) to future climate projections relies on the assumption that model biases estimated during the historical period remain stationary in the future(Switanek *et al.*, 2017). However, future climate data are inherently non-stationary(Switanek *et al.*, 2017; Vrac *et al.*, 2025). To assess whether non-stationarity in the projections is preserved after bias correction, we evaluated PEAK SWE change signals before and after correction for each GCM. Fig. 5(b) illustrates the GFDL-ESM4 model as a case study. The bias-corrected SWE closely follows the raw GCM output over the 2015–2099 projection period, with a correlation of 0.989, indicating that the temporal evolution is well preserved. For the same period, the linear trend in SWE from the raw GCM was −0.305 mm yr^{-1}, while the bias-corrected series exhibited a slightly stronger decline of −0.375 mm yr^{-1}. This minor difference results from the time-step-specific correction, which adjusts systematic biases without altering the overall climate change signal. These results demonstrate that the bias correction method effectively reduces systematic errors while retaining non-stationary climate change signals, thereby mitigating limitations commonly associated with the stationarity assumption in traditional bias correction approaches.

https://doi.org/10.5194/essd-2026-303
Preprint. Discussion started: 30 June 2026

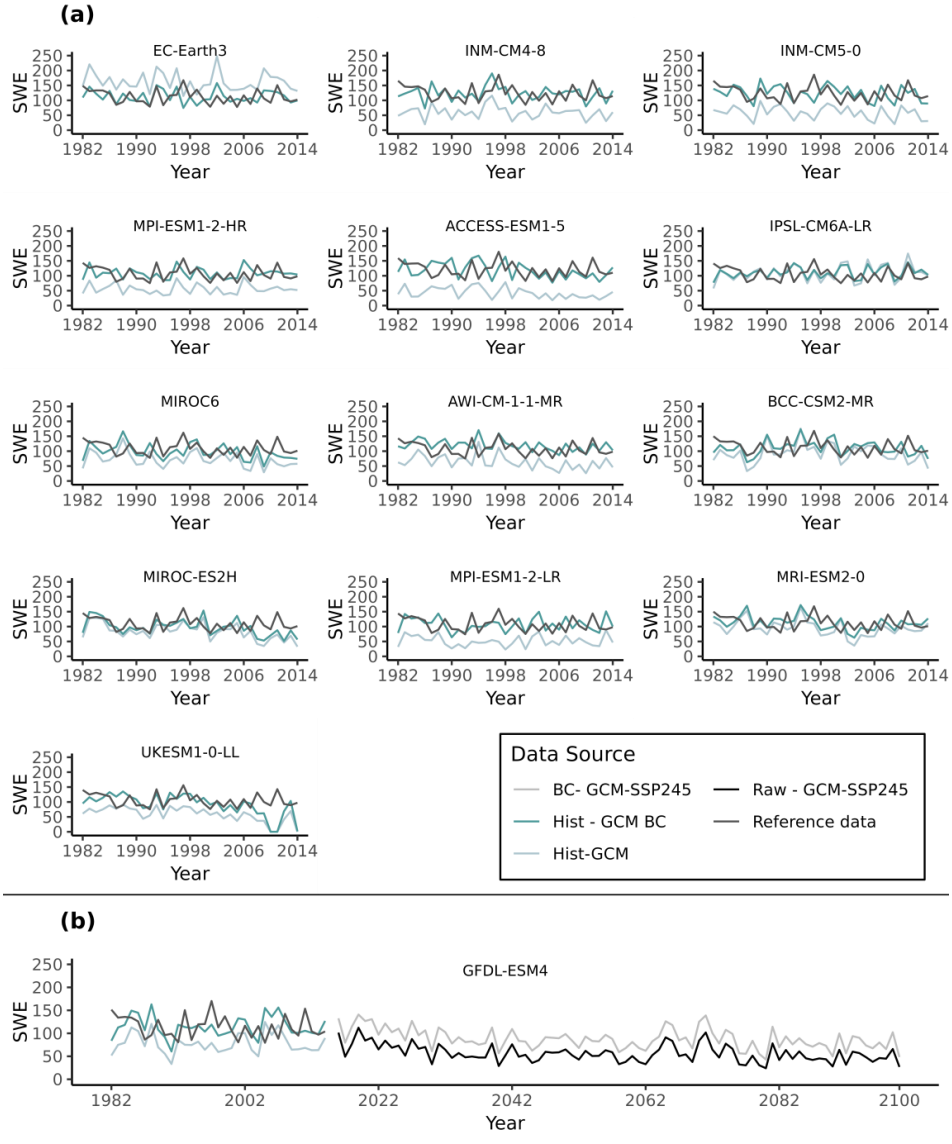

Fig. 5. (a) Comparison of snow water equivalent (SWE) across the western U.S. (1982–2014) for 14 climate models showing reference data (black), raw GCM outputs (gray), and bias-corrected GCM outputs (green). Panel (b) shows the SWE projection from 2015 to 2099 for GFDL-ESM4 as an example, illustrating that time-step-specific bias correction preserves the temporal evolution and long-term climate change trend despite non-stationary biases.

To complement the domain-wide ensemble assessment, bias-correction performance was also evaluated at the pixel level. Fig. 6 presents empirical cumulative distribution functions (CDFs) of daily snow water equivalent (SWE) at four representative grid cells selected to illustrate contrasting bias regimes. In overestimation cases (EC-Earth3; Fig. 6(a)–(b)), the raw GCM CDF is shifted

https://doi.org/10.5194/essd-2026-303
Preprint. Discussion started: 30 June 2026

substantially to the right of the reference distribution, indicating higher simulated SWE than observed, with mean biases of +91 mm and +66.2 mm. In underestimation cases (INM-CM5-0; Fig. 6(c)–(d)), the raw GCM CDF is shifted to the left, reflecting lower simulated SWE relative to the reference dataset, with mean biases of −180.4 mm and −14.9 mm. Following bias correction, the CDFs align closely with the reference distribution in all four cases, demonstrating that the quantile-mapping approach effectively reduces systematic biases across a wide range of bias magnitudes and directions. These pixel-level results are consistent with the ensemble-mean improvements shown in Fig. 5 and indicate that the bias-correction procedure performs robustly across individual locations and climate models, thereby reinforcing confidence in the spatial consistency of the ClimAVA-SWE dataset.

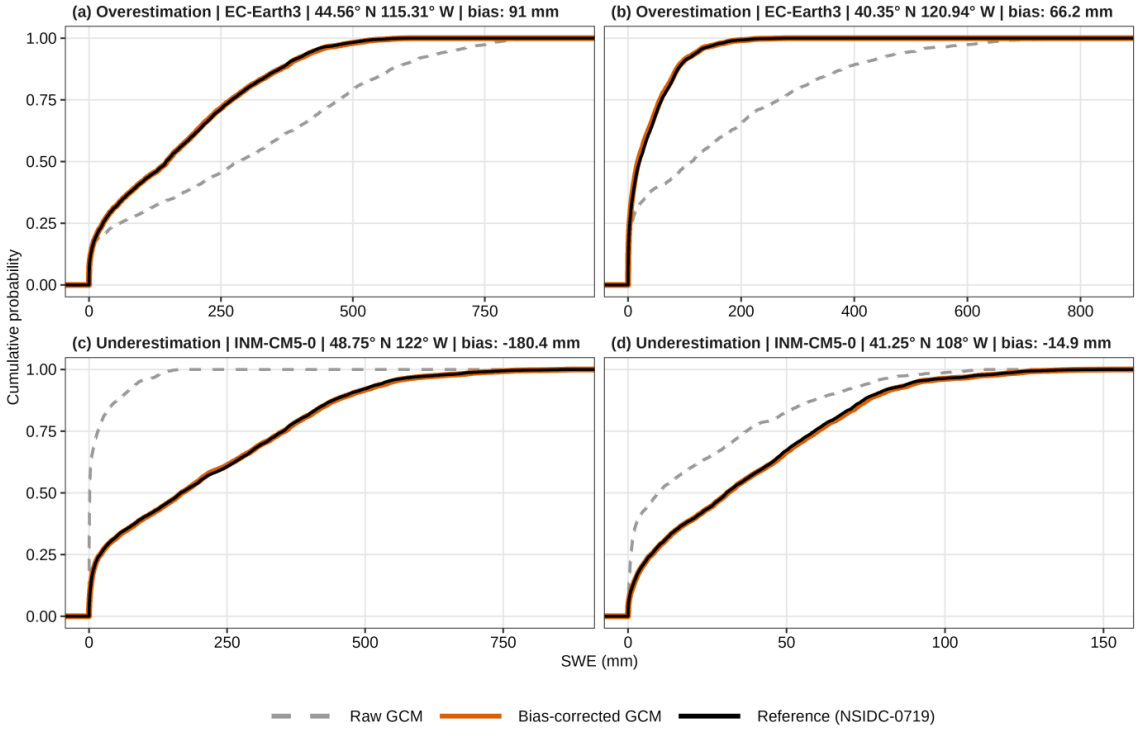

Fig. 6. Empirical cumulative distribution functions (CDFs) of daily snow water equivalent (SWE) at four randomly selected locations across the western United States illustrating the effect of quantile-mapping bias correction. Panels (a) and (b) show locations where the raw GCM output from EC-Earth3 overestimates SWE relative to the reference dataset. Panels (c) and (d) show locations where the raw GCM output from INM-CM5-0 underestimates SWE. In all panels, the gray dashed line represents the raw GCM output, the black line represents the reference dataset (NSIDC-0719), and the green line represents the bias-corrected GCM output.

Supplementary spatial maps illustrating the distribution and magnitude of these metrics—both before and after correction—are available in the supplementary material.

https://doi.org/10.5194/essd-2026-303
Preprint. Discussion started: 30 June 2026

4.Downscaled SWE Assessment

To evaluate the consistency and realism of the downscaled SWE projections, we first used the annual peak SWE metric to assess the dataset across four representative basins in the western U.S. Table. 2, examining basin-scale snowpack behavior and inter-model variability. While these basins cover only a portion of the domain, they serve as useful case studies for testing the physical plausibility of the results (Fig. 7(a)). Across all four basins—Colorado, Great Salt Lake, Sacramento–San Joaquin, and Willamette—the downscaled historical simulations successfully capture reference peak SWE patterns. The ensemble mean and long-term trends closely align with the reference data, while extreme values remain consistently within the ensemble range. Future projections indicate a clear decline in annual peak SWE under all three SSPs, with the steepest reductions occurring under the highest emissions scenario (SSP585).

To further assess model performance, we produced spatial difference maps (Fig. 7(b)) showing the mean bias between the historical run of each downscaled GCM and the reference dataset (model – reference) for 1982–2014, corresponding to the availability of reference data. Most GCMs exhibit systematic underestimation of annual peak SWE across high-elevation areas of the Rocky Mountains, spanning the Southern, Central, and Northern Rockies in Colorado, Utah, Wyoming, and Idaho. In contrast, AWI-CM-1-1-MR shows widespread overestimation across the domain. EC-Earth3 displays a mixed pattern, with both over- and underestimation depending on location. GFDL-ESM4 tends to overestimate annual peak SWE in the snow-dominated high-elevation regions of the Sierra Nevada, Cascade Range, and Olympic Mountains in California, Oregon, and Washington, while underestimating elsewhere. INM-CM4-8, INM-CM5-0, and MPI-ESM1-2-LR consistently underestimate annual peak SWE across most of the region, and MIROC-ES2H and MIROC also exhibit widespread underestimation. Overall, EC-Earth3 and GFDL-ESM4 show the smallest biases relative to the reference dataset, reflecting better performance in capturing reference data SWE patterns across the western U.S. However, in the final panel, the deviation from the ensemble mean exhibits smaller, more moderate biases across the domain, with a consistent tendency toward underestimation rather than overestimation.

https://doi.org/10.5194/essd-2026-303
Preprint. Discussion started: 30 June 2026

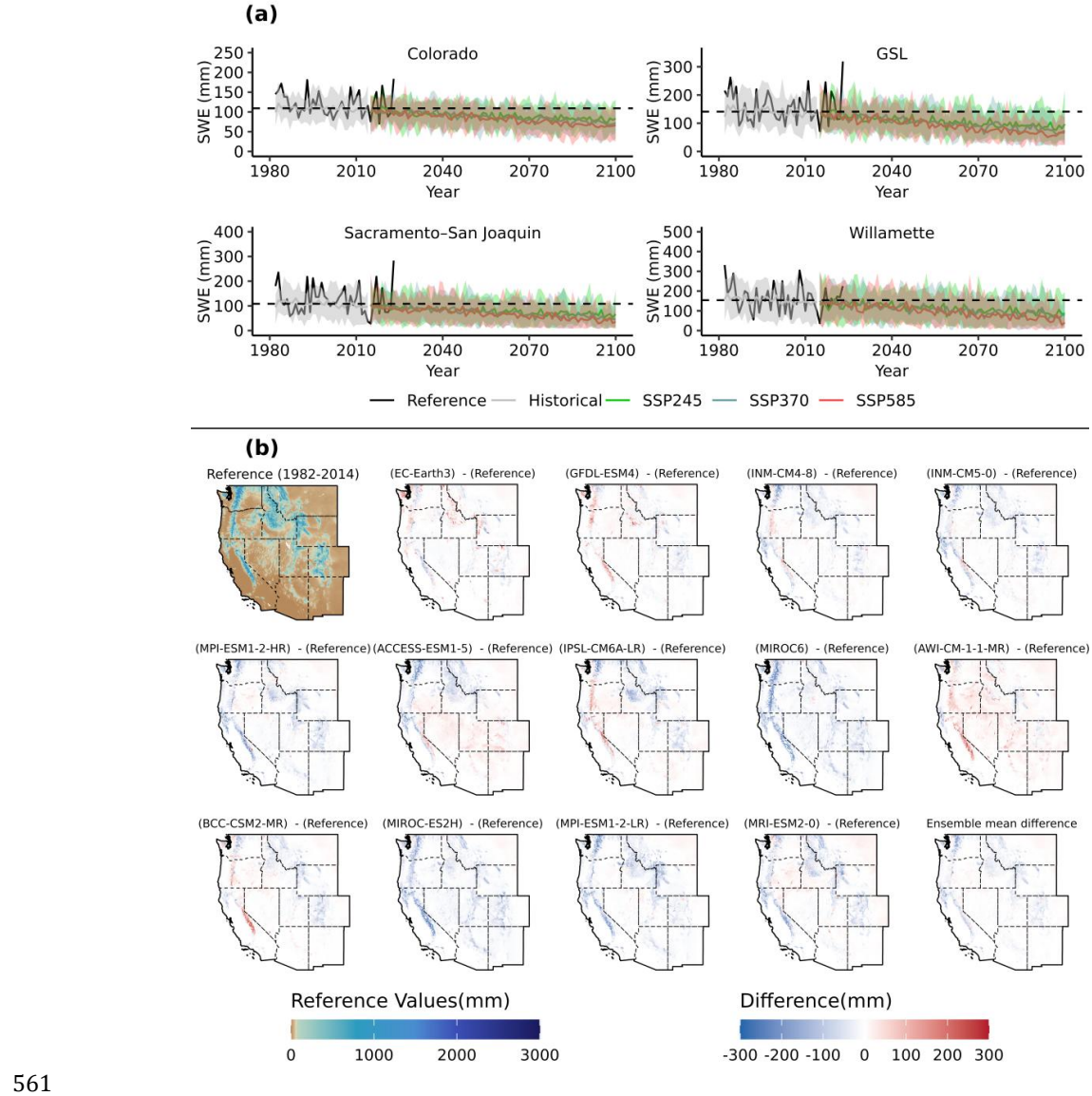

Fig. 7. (a) Annual peak Snow Water Equivalent (SWE) from 1981 to 2100 across four western U.S. basins: Colorado, Great Salt Lake (GSL), Sacramento–San Joaquin, and Willamette, Projections are shown for historical and future periods under three CMIP6 scenarios (SSP245, SSP370, and SSP585), solid lines indicate the multi-model ensemble mean and shaded areas reflect the inter-model range (minimum to maximum) across the 14 CMIP6 GCMs and (b) Spatial difference maps showing the mean bias between each GCM and the reference dataset for 1982–2014, with the last panel representing the ensemble mean.

We next examine the spatial evolution of peak SWE changes relative to the historical baseline under SSP585 (Fig. 8). The reference period (1982–2014), shown in Fig. 8(a), depicts the spatial

https://doi.org/10.5194/essd-2026-303
Preprint. Discussion started: 30 June 2026

distribution of mean annual peak SWE, with substantial snow accumulation concentrated at higher elevations across the western United States. The three future panels depict differences in peak SWE relative to this baseline (future minus reference): near-term (2015–2040) in Fig. 8(b), mid-century (2041–2070) in Fig. 8(c), and late century (2071–2100) in Fig. 8(d). Across all future periods, negative changes dominate, indicating widespread reductions in peak SWE under the high-emission scenario. In the near future (Fig. 8(b)), decreases are already apparent across much of the region, though their magnitude is generally modest and spatially heterogeneous. By mid-century (Fig. 8(c)), the magnitude and spatial extent of negative differences increase substantially, particularly across major mountain systems. By late century (Fig. 8(d)), strong and widespread negative departures relative to the reference period prevail, indicating pronounced losses in peak SWE across nearly all snow-dominated regions.

Regionally, the Sierra Nevada exhibits consistent negative changes beginning in the near future, which intensify through mid- and late-century, indicating substantial reductions in snowpack. The Cascade Range—from Washington through Oregon into northern California—shows a similar pattern, with increasingly strong negative differences, especially at lower and mid-elevations. In the central Rocky Mountains, including the Sawatch and Front Range of Colorado, negative changes become more pronounced over time, reflecting steady declines in SWE. Comparable patterns are observed in the Wasatch Range in Utah and in the Teton and Wind River ranges in Wyoming, where increasingly negative differences indicate substantial reductions and the progressive loss of snowpack. These spatial patterns are consistent with previous downscaled GCM-based studies that project widespread declines in SWE across the western U.S. under climate scenarios(Maloney *et al.*, no date; Mccrary and Mearns, no date; Demaria *et al.*, 2016).

https://doi.org/10.5194/essd-2026-303
Preprint. Discussion started: 30 June 2026

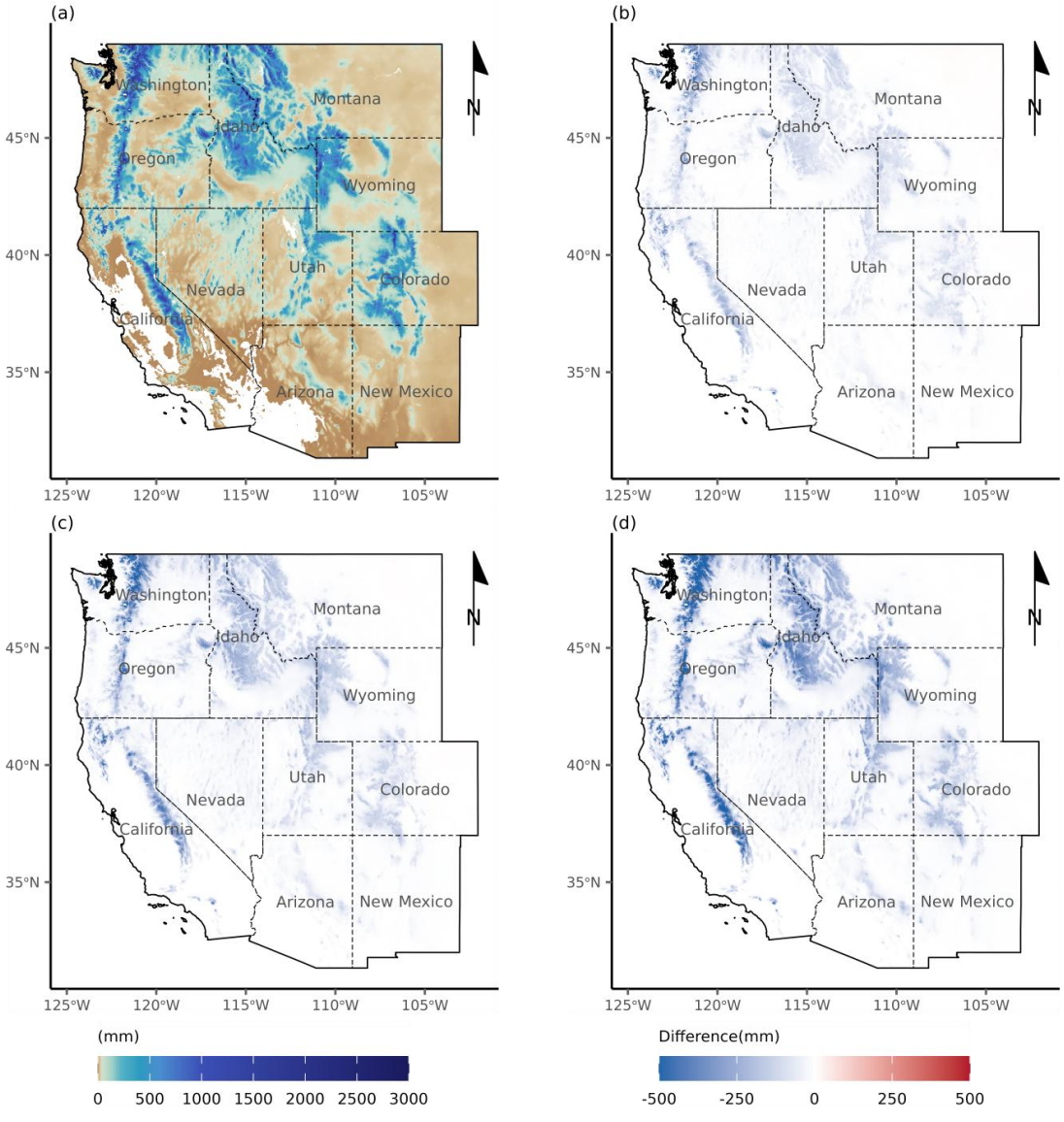

Fig. 8. Spatial evolution of mean annual peak snow water equivalent (SWE) across the western United States under the high-emission scenario SSP585. Panel (a) shows the spatial distribution of mean peak SWE during the reference period (1982–2014). Panels (b)–(d) display changes in peak SWE relative to the reference period (future minus reference) for the near-term (2015–2040) in (b), mid-century (2041–2070) in (c), and late-century (2071–2100) in (d).

5. Strengths, Limitations and Uncertainties

In summary, SPID-SWE has demonstrated strong capability in downscaling snow water equivalent (SWE) data by treating each pixel independently in both space and time. This pixel-based, double-

https://doi.org/10.5194/essd-2026-303
Preprint. Discussion started: 30 June 2026

model approach ensures that each location is processed without influence from neighboring pixels or adjacent days, allowing for an accurate representation of spatial and temporal dynamics. The model is computationally efficient (see Section 2.5. in Methods) and accurate, and as new generations of GCMs improve the representation of temporal SWE dynamics, SPID-SWE is well-positioned to downscale these datasets with precision. This capability is essential for generating high-resolution future climate projections that support informed local decision-making in a rapidly changing climate. However, the efficacy of SPID-SWE depends heavily on the quality of the coarse input data. If the original dataset lacks realistic spatial or temporal patterns, the downscaling will carry over those limitations. Current GCMs still exhibit significant temporal biases in SWE outputs, most notably an overrepresentation of zero-snow days. Despite this, GCMs generally reproduce annual peak SWE reasonably well, especially after bias correction, and trends derived from peak SWE align closely with reference datasets, reinforcing confidence in their broader applicability.

Several additional sources of uncertainty should be noted. The model is trained using NSIDC-0719 dataset, which itself contains uncertainties because it is derived from in-situ measurements, and gridded meteorological inputs from PRISM. Although PRISM incorporates elevation and provides high-quality climate fields, precipitation and snow estimates in complex terrain can still exhibit substantial uncertainty due to sparse observations and strong spatial gradients in mountainous regions(Henn *et al.*, 2018). Consequently, uncertainties in the reference SWE dataset propagate into the downscaled product. SPID-SWE primarily relies on coarse-resolution SWE predictors and spatial context rather than explicit land surface variables such as topography and vegetation. At 4-km resolution, these factors can influence snow accumulation and melt processes, particularly in mountainous regions of the western United States. Vegetation canopy, complex terrain, and local energy balance processes can modify snow distribution and melt timing(Ikeda *et al.*, 2021).

Although terrain attributes are not explicitly incorporated, their effects are implicitly captured through the reference datasets (e.g., NSIDC-0719), which rely on PRISM outputs and other auxiliary covariates. Training models independently for each pixel allows these terrain characteristics to be effectively represented without additional covariates, reducing model complexity and improving computational efficiency. The strong validation performance of SPID-SWE in high-elevation, complex terrain supports this approach (Fig. 2).

Glacierized areas represent an additional source of uncertainty in high-elevation regions, particularly in the Cascade Range and northern Rockies. The downscaled SWE dataset produced here captures seasonal snowpack variability at annual timescales, rather than multi-year accumulation. This limitation arises from both the reference dataset and the driving climate model outputs. The reference dataset, NSIDC-0719(Zeng, Broxton and Dawson, 2018), reconstructs SWE using in-situ measurements and gridded temperature and precipitation from PRISM(Daly, Smith and Olson, 2015), which itself provides no snow storage information. Consequently, NSIDC-0719 captures only seasonal snow and does not explicitly represent glacier mass or long-term ice dynamics. Similarly, the CMIP6 GCM outputs used to drive the downscaling represent seasonal

https://doi.org/10.5194/essd-2026-303
Preprint. Discussion started: 30 June 2026

snow as part of the land surface scheme, without explicit glacier storage or multi-year accumulation(O'Neill *et al.*, 2016; Luojus *et al.*, 2021). Glacierized grid cells are therefore effectively treated as seasonal snow-covered areas, and the resulting SWE estimates primarily reflect the seasonal snow component rather than total frozen water storage.

The random forest algorithm used in SPID-SWE is inherently limited in extrapolation beyond the range of the training data. Extremely high SWE values outside the historical record may be underestimated, although the multi-decadal training dataset captures a wide range of climatic variability. Examination of peak SWE in future projections, following bias correction, indicates that simulated maxima remain within the historical range (e.g., Fig. 5(b)). However, at finer resolutions, extremes may not be fully captured, and dynamical downscaling approaches may be required to resolve localized snow increases in high-elevation regions under enhanced winter precipitation(Notarnicola, 2020; Kawase *et al.*, 2021).

Data Availability

ClimAVA-SWE dataset provides daily snow water equivalent (SWE) projections at ~4 km spatial resolution for 14 CMIP6 global climate models (GCMs; see Table 1), covering both historical and future scenarios under three Shared Socioeconomic Pathways (SSP245, SSP370, and SSP585). Historical simulations span January 1, 1981, to December 31, 2014, while future scenarios extend from January 1, 2015, to December 31, 2100. Each year in the dataset contains exactly 365 days, with leap days excluded for consistency, and data are provided in NetCDF4 format. This dataset covers 11 western U.S. states, including Washington, Oregon, California, Idaho, Nevada, Utah, Arizona, Montana, Wyoming, Colorado, and New Mexico. The ClimAVA-SWE dataset is publicly available through the Harvard Dataverse and can be accessed via its official repository at https://doi.org/10.7910/DVN/SCD2VT (Khoshnood Motlagh, de Lima Moraes and Smith, 2026)

Code Availability

All code required to reproduce the dataset creation methodology, as well as the analyses used to generate the results, is publicly available on our GitHub repository:

https://github.com/ClimAVA/ClimaAVA-SWE

Funding

This research was supported by the Utah Agricultural Experiment Station, Utah State University, and approved as journal paper number #9938, the Utah Climate Center, and the Center for High-Performance Computing at the University of Utah.

https://doi.org/10.5194/essd-2026-303
Preprint. Discussion started: 30 June 2026

Author Contributions

Sajad Khoshnood Motlagh conceived the study; designed and implemented the SPID-SWE framework; developed the ClimAVA-SWE dataset; performed data processing, analysis, and validation; and led the writing of the manuscript.

Andre Geraldo de Lima Moraes co-designed and co-implemented the SPID-SWE framework, provided continuous supervision and guidance throughout the study, and contributed to methodological development, interpretation of results, and manuscript revisions.

Kayla Smith contributed to dataset validation.

Wei Zhang, Sarah Null, Anna Miller, and Yoshimitsu Chikamoto reviewed the manuscript and provided scientific feedback and suggestions.

All authors discussed the results and approved the final manuscript.

Competing Interests

There are no known conflicts of interest associated with this publication.

Figures

Figures and Tables are provided as separate files.

References

Abatzoglou, J.T. and Brown, T.J. (2012) 'A comparison of statistical downscaling methods suited for wildfire applications', *International Journal of Climatology*, 32(5), pp. 772–780. Available at: https://doi.org/10.1002/joc.2312.

Alder, J.R. and Hostetler, S.W. (2019) 'The Dependence of Hydroclimate Projections in Snow-Dominated Regions of the Western United States on the Choice of Statistically Downscaled Climate Data', *Water Resources Research*, 55(3), pp. 2279–2300. Available at: https://doi.org/10.1029/2018WR023458.

America, N. *et al.* (no date) 'Twenty-First-Century Projections of Snowfall and Winter Severity across Central-Eastern'. Available at: https://doi.org/10.1175/JCLI-D-13-00520.s1.

Ashfaq, M. *et al.* (2016) 'High-resolution ensemble projections of near-term regional climate over the continental United States', *Journal of Geophysical Research*, 121(17), pp. 9943–9963. Available at: https://doi.org/10.1002/2016JD025285.

https://doi.org/10.5194/essd-2026-303
Preprint. Discussion started: 30 June 2026

699 Attique, R., Rientjes, T. and Booij, M. (2023) 'Comparison between statistical and dynamical
700 downscaling of rainfall over the Gwadar-Ormara basin, Pakistan', *Meteorological Applications*,
701 30(5), pp. 1–19. Available at: https://doi.org/10.1002/met.2151.

702 Baghanam, A.H. *et al.* (2024) 'Improving the statistical downscaling performance of climatic
703 parameters with convolutional neural networks', *Journal of Water and Climate Change*, 15(4), pp.
704 1772–1796. Available at: https://doi.org/10.2166/wcc.2024.592.

705 Baño-Medina, J. (2020) 'Understanding Deep Learning Decisions in Statistical Downscaling
706 Models', *ACM International Conference Proceeding Series*. Association for Computing Machinery,
707 pp. 79–85. Available at: https://doi.org/10.1145/3429309.3429321.

708 Banõ-Medina, J. *et al.* (2022) 'Downscaling multi-model climate projection ensembles with deep
709 learning (DeepESD): Contribution to CORDEX EUR-44', *Geoscientific Model Development*, 15(17),
710 pp. 6747–6758. Available at: https://doi.org/10.5194/gmd-15-6747-2022.

711 Brown, L.C. and Duguay, C.R. (2010) 'The response and role of ice cover in lake-climate
712 interactions', *Progress in Physical Geography*, 34(5), pp. 671–704. Available at:
713 https://doi.org/10.1177/0309133310375653.

714 Brown, R.D. and Mote, P.W. (2009) 'The response of Northern Hemisphere snow cover to a
715 changing climate', *Journal of Climate*, 22(8), pp. 2124–2145. Available at:
716 https://doi.org/10.1175/2008JCLI2665.1.

717 Brutel-Vuilmet, C., Ménégoz, M. and Krinner, G. (2013) 'An analysis of present and future seasonal
718 Northern Hemisphere land snow cover simulated by CMIP5 coupled climate models', *Cryosphere*,
719 pp. 67–80. Available at: https://doi.org/10.5194/tc-7-67-2013.

720 Callaghan, T. V. *et al.* (2011) 'The changing face of arctic snow cover: A synthesis of observed and
721 projected changes', *Ambio*, 40(SUPPL. 1), pp. 17–31. Available at:
722 https://doi.org/10.1007/s13280-011-0212-y.

723 Cannon, A.J., Sobie, S.R. and Murdock, T.Q. (2015) 'Bias correction of GCM precipitation by quantile
724 mapping: How well do methods preserve changes in quantiles and extremes?', *Journal of Climate*,
725 28(17), pp. 6938–6959. Available at: https://doi.org/10.1175/JCLI-D-14-00754.1.

726 Chen, S.T., Yu, P.S. and Tang, Y.H. (2010) 'Statistical downscaling of daily precipitation using
727 support vector machines and multivariate analysis', *Journal of Hydrology*, 385(1–4), pp. 13–22.
728 Available at: https://doi.org/10.1016/j.jhydrol.2010.01.021.

729 Cho, E. and Jacobs, J.M. (2020) 'Extreme Value Snow Water Equivalent and Snowmelt for
730 Infrastructure Design Over the Contiguous United States', *Water Resources Research*, 56(10).
731 Available at: https://doi.org/10.1029/2020WR028126.

https://doi.org/10.5194/essd-2026-303
Preprint. Discussion started: 30 June 2026

Christensen, N.S. and Lettenmaier, D.P. (2007) 'A multimodel ensemble approach to assessment of climate change impacts on the hydrology and water resources of the Colorado River Basin', *Hydrology and Earth System Sciences*, 11(4), pp. 1417–1434. Available at: https://doi.org/10.5194/hess-11-1417-2007.

Cody Ratterman *et al.* (2025) 'Improving CFSv2 Snow Water Equivalent Forecasts in the Colorado River Basin with Generalized Analog Regression Downscaling', *Weather and Forecasting*, 40(11), pp. 2381–32389. Available at: https://doi.org/https://doi.org/10.1175/WAF-D-23-0196.1.

Daly, C., Smith, J.I. and Olson, K. V. (2015) 'Mapping atmospheric moisture climatologies across the conterminous United States', *PLoS ONE*, 10(10). Available at: https://doi.org/10.1371/journal.pone.0141140.

Damiani, A. *et al.* (2025) 'Projecting future snow changes at kilometer scale for adaptation using machine learning and a CMIP6 multi-model ensemble', *Science of the Total Environment*, 964. Available at: https://doi.org/10.1016/j.scitotenv.2025.178606.

Demaria, E.M.C. *et al.* (2016) 'The effects of climate change on seasonal snowpack and the hydrology of the Northeastern and Upper Midwest United States', *Journal of Climate*, 29(18), pp. 6527–6541. Available at: https://doi.org/10.1175/JCLI-D-15-0632.1.

Derksen, C. *et al.* (2012) 'Variability and change in the Canadian cryosphere', *Climatic Change*, 115(1), pp. 59–88. Available at: https://doi.org/10.1007/s10584-012-0470-0.

Diffenbaugh, N.S., Scherer, M. and Ashfaq, M. (2013) 'Response of snow-dependent hydrologic extremes to continued global warming', *Nature Climate Change*, 3(4), pp. 379–384. Available at: https://doi.org/10.1038/nclimate1732.

Ekström, M. *et al.* (2016) 'The method of producing climate change datasets impacts the resulting policy guidance and chance of mal-adaptation', *Climate Services*, 4, pp. 13–29. Available at: https://doi.org/10.1016/j.cliser.2016.09.003.

Enayati, M. *et al.* (2021) 'Bias correction capabilities of quantile mapping methods for rainfall and temperature variables', *Journal of Water and Climate Change*, 12(2), pp. 401–419. Available at: https://doi.org/10.2166/wcc.2020.261.

Eum, H. Il, Gupta, A. and Dibike, Y. (2020) 'Effects of univariate and multivariate statistical downscaling methods on climatic and hydrologic indicators for Alberta, Canada', *Journal of Hydrology*, 588(May), p. 125065. Available at: https://doi.org/10.1016/j.jhydrol.2020.125065.

Eyring, V. *et al.* (2016) 'Overview of the Coupled Model Intercomparison Project Phase 6 (CMIP6) experimental design and organization', *Geoscientific Model Development*, 9(5), pp. 1937–1958. Available at: https://doi.org/10.5194/gmd-9-1937-2016.

https://doi.org/10.5194/essd-2026-303
Preprint. Discussion started: 30 June 2026

765 Fassnacht, S.R. *et al.* (2016) 'Snow and albedo climate change impacts across the United States
766 Northern Great Plains', *Cryosphere*, 10(1), pp. 329–339. Available at: https://doi.org/10.5194/tc-
767 10-329-2016.

768 Fowler, H.J., Blenkinsop, S. and Tebaldi, C. (2007) 'Linking climate change modelling to impacts
769 studies: Recent advances in downscaling techniques for hydrological modelling', *International*
770 *Journal of Climatology*, pp. 1547–1578. Available at: https://doi.org/10.1002/joc.1556.

771 Gelaro, R. *et al.* (2017) 'The modern-era retrospective analysis for research and applications,
772 version 2 (MERRA-2)', *Journal of Climate*, 30(14), pp. 5419–5454. Available at:
773 https://doi.org/10.1175/JCLI-D-16-0758.1.

774 Harris, R.M.B. *et al.* (2014) 'Climate projections for ecologists', *Wiley Interdisciplinary Reviews:*
775 *Climate Change*, pp. 621–637. Available at: https://doi.org/10.1002/wcc.291.

776 Henn, B. *et al.* (2018) 'An assessment of differences in gridded precipitation datasets in complex
777 terrain', *Journal of Hydrology*, 556, pp. 1205–1219. Available at:
778 https://doi.org/10.1016/j.jhydrol.2017.03.008.

779 Ikeda, K. *et al.* (2021) 'Snowfall and snowpack in the Western U.S. as captured by convection
780 permitting climate simulations: current climate and pseudo global warming future climate',
781 *Climate Dynamics*, 57(7–8), pp. 2191–2215. Available at: https://doi.org/10.1007/s00382-021-
782 05805-w.

783 Jörg-Hess, S. *et al.* (2014) 'Homogenisation of a gridded snow water equivalent climatology for
784 Alpine terrain: Methodology and applications', *Cryosphere*, 8(2), pp. 471–485. Available at:
785 https://doi.org/10.5194/tc-8-471-2014.

786 Kapnick, S. and Hall, A. (2012) 'Causes of recent changes in western North American snowpack',
787 *Climate Dynamics*, 38(9–10), pp. 1885–1899. Available at: https://doi.org/10.1007/s00382-011-
788 1089-y.

789 Kawase, H. *et al.* (2021) 'Regional Characteristics of Future Changes in Snowfall in Japan under
790 RCP2.6 and RCP8.5 Scenarios', *Scientific Online Letters on the Atmosphere*, 17, pp. 1–7. Available at:
791 https://doi.org/10.2151/SOLA.2021-001.

792 Keller, A.A. *et al.* (2022) 'Downscaling approaches of climate change projections for watershed
793 modeling: Review of theoretical and practical considerations', *PLOS Water*, 1(9), p. e0000046.
794 Available at: https://doi.org/10.1371/journal.pwat.0000046.

795 Khoshnood Motlagh, S. and de Lima Moraes, A.G. (2025) *Climate data for adaptation and*
796 *vulnerability assessments — northwest*. Available at:
797 https://doi.org/https://doi.org/10.26050/WDCC/ClimAVA-NW.

https://doi.org/10.5194/essd-2026-303
Preprint. Discussion started: 30 June 2026

798 Khoshnood Motlagh, S., de Lima Moraes, A.G. and Smith, K. (2026) *ClimAVA-SWE: A High-*
799 *Resolution CMIP6-Based Snow Water Equivalent Dataset for the Western United States*, *Harvard*
800 *Dataverse. https://doi.org/10.7910/DVN/SCD2VT*.

801 Klos, P.Z., Link, T.E. and Abatzoglou, J.T. (2014a) 'Extent of the rain-snow transition zone in the
802 western U.S. under historic and projected climate', *Geophysical Research Letters*, 41(13), pp. 4560–
803 4568. Available at: https://doi.org/10.1002/2014GL060500.

804 Klos, P.Z., Link, T.E. and Abatzoglou, J.T. (2014b) 'Extent of the rain-snow transition zone in the
805 western U.S. under historic and projected climate', *Geophysical Research Letters*, 41(13), pp. 4560–
806 4568. Available at: https://doi.org/10.1002/2014GL060500.

807 Knowles, N. (2015) 'Trends in snow cover and related quantities at weather stations in the
808 conterminous United States', *Journal of Climate*, 28(19), pp. 7518–7528. Available at:
809 https://doi.org/10.1175/JCLI-D-15-0051.1.

810 Krasting, J.P. *et al.* (2013) 'Future changes in northern hemisphere snowfall', *Journal of Climate*,
811 26(20), pp. 7813–7828. Available at: https://doi.org/10.1175/JCLI-D-12-00832.1.

812 L Westerling, B.A. *et al.* (no date) *CLIMATE AND WILDFIRE IN THE WESTERN UNITED STATES*.

813 Lanzante, J.R. *et al.* (2018) 'Some pitfalls in statistical downscaling of future climate', *Bulletin of the*
814 *American Meteorological Society*, 99(4), pp. 791–803. Available at:
815 https://doi.org/10.1175/BAMS-D-17-0046.1.

816 Li, D. *et al.* (2017) 'How much runoff originates as snow in the western United States, and how will
817 that change in the future?', *Geophysical Research Letters*, 44(12), pp. 6163–6172. Available at:
818 https://doi.org/10.1002/2017GL073551.

819 Li, H., Sheffield, J. and Wood, E.F. (2010) 'Bias correction of monthly precipitation and temperature
820 fields from Intergovernmental Panel on Climate Change AR4 models using equidistant quantile
821 matching', *Journal of Geophysical Research Atmospheres*, 115(10). Available at:
822 https://doi.org/10.1029/2009JD012882.

823 Li, Z. *et al.* (2025) 'High-resolution snow water equivalent estimation derived from downscaled
824 snow depth and non-constant snow density in Chinese Altai Mountains', *Journal of Hydrology*, 661.
825 Available at: https://doi.org/10.1016/j.jhydrol.2025.133708.

826 Liaw, A. and Wiener, M. (2002) 'Classification and Regression by randomForest', *R News*, 2(3), pp.
827 18–22.

828 de Lima Moraes, A.G. and Khoshnood Motlagh, S. (2024a) 'Climate data for adaptation and
829 vulnerability assessments — southwest'. World Data Center for Climate (WDCC) at DKRZ.
830 Available at: https://doi.org/10.26050/WDCC/ClimAVA-SW.

https://doi.org/10.5194/essd-2026-303
Preprint. Discussion started: 30 June 2026

de Lima Moraes, A.G. and Khoshnood Motlagh, S. (2024b) 'The Climate Data for Adaptation and Vulnerability Assessments and the Spatial Interactions Downscaling Method', *Scientific Data* , 11(1). Available at: https://doi.org/10.1038/s41597-024-03995-6.

de Lima Moraes, A.G. and Motlagh, S.K. (2024) 'The Climate Data for Adaptation and Vulnerability Assessments and the Spatial Interactions Downscaling Method', *Scientific data*, 11(1), p. 1157. Available at: https://doi.org/10.1038/s41597-024-03995-6.

Liu, Z.L. *et al.* (2010) 'Application of artificial neural networks in global climate change and ecological research: An overview', *Chinese Science Bulletin*, pp. 3853–3863. Available at: https://doi.org/10.1007/s11434-010-4183-3.

Livneh, B. *et al.* (no date) 'A Long-Term Hydrologically Based Dataset of Land Surface Fluxes and States for the Conterminous United States: Update and Extensions* , #'. Available at: https://doi.org/10.1175/JCLI-D-12.

Luojus, K. *et al.* (2021) 'GlobSnow v3.0 Northern Hemisphere snow water equivalent dataset', *Scientific Data*, 8(1). Available at: https://doi.org/10.1038/s41597-021-00939-2.

Mahanama, S. *et al.* (2012) 'Soil moisture, snow, and seasonal streamflow forecasts in the United States', *Journal of Hydrometeorology*, 13(1), pp. 189–203. Available at: https://doi.org/10.1175/JHM-D-11-046.1.

Maloney, E.D. *et al.* (no date) 'North American Climate in CMIP5 Experiments: Part III: Assessment of Twenty-First-Century Projections*'. Available at: https://doi.org/10.1175/JCLI-D.

Matiu, M. and Hanzer, F. (2022) 'Bias adjustment and downscaling of snow cover fraction projections from regional climate models using remote sensing for the European Alps', *Hydrology and Earth System Sciences*, 26(12), pp. 3037–3054. Available at: https://doi.org/10.5194/hess-26-3037-2022.

Maurer, E.P. (2007) 'Uncertainty in hydrologic impacts of climate change in the Sierra Nevada, California, under two emissions scenarios', *Climatic Change*, 82(3–4), pp. 309–325. Available at: https://doi.org/10.1007/s10584-006-9180-9.

Maurer, E.P. *et al.* (2010) 'The utility of daily large-scale climate data in the assessment of climate change impacts on daily streamflow in California', *Hydrology and Earth System Sciences*, 14(6), pp. 1125–1138. Available at: https://doi.org/10.5194/hess-14-1125-2010.

Mccrary, R.R. and Mearns, L.O. (no date) 'Quantifying and Diagnosing Sources of Uncertainty in Midcentury Changes in North American Snowpack from NARCCAP'. Available at: https://doi.org/10.1175/JHM-D-18-0248.s1.

https://doi.org/10.5194/essd-2026-303
Preprint. Discussion started: 30 June 2026

Mearns, L.O. *et al.* (2012) 'The north american regional climate change assessment program overview of phase i results', *Bulletin of the American Meteorological Society*, 93(9), pp. 1337–1362. Available at: https://doi.org/10.1175/BAMS-D-11-00223.1.

Michel, A. *et al.* (2024) 'SnowQM 1.0: a fast R package for bias-correcting spatial fields of snow water equivalent using quantile mapping', *Geoscientific Model Development*, 17(24), pp. 8969–8988. Available at: https://doi.org/10.5194/gmd-17-8969-2024.

Mote, P.W. *et al.* (2005) *DECLINING MOUNTAIN SNOWPACK IN WESTERN NORTH AMERICA**. Available at: http://wlapwww.gov.bc.ca/rfc/.

Mote, P.W. *et al.* (2018) 'Dramatic declines in snowpack in the western US', *npj Climate and Atmospheric Science*, 1(1). Available at: https://doi.org/10.1038/s41612-018-0012-1.

Muñoz-Sabater, J. *et al.* (2021) 'ERA5-Land: A state-of-the-art global reanalysis dataset for land applications', *Earth System Science Data*, 13(9), pp. 4349–4383. Available at: https://doi.org/10.5194/essd-13-4349-2021.

Musselman, K.N. *et al.* (2017) 'Slower snowmelt in a warmer world', *Nature Climate Change*, 7(3), pp. 214–219. Available at: https://doi.org/10.1038/nclimate3225.

Notarnicola, C. (2020) 'Hotspots of snow cover changes in global mountain regions over 2000–2018', *Remote Sensing of Environment*, 243. Available at: https://doi.org/10.1016/j.rse.2020.111781.

NRCS, N.R.C.S. (2026) *Snow Telemetry (SNOTEL) data and products*, *United States Department of Agriculture (USDA). Available at: https://www.nrcs.usda.gov/wps/portal/wcc/home/snowClimateMonitoring/snowpack/snotelSnopackProducts/*.

O'Neill, B.C. *et al.* (2016) 'The Scenario Model Intercomparison Project (ScenarioMIP) for CMIP6', *Geoscientific Model Development*, 9(9), pp. 3461–3482. Available at: https://doi.org/10.5194/gmd-9-3461-2016.

Painter, T.H. *et al.* (2016) 'The Airborne Snow Observatory: Fusion of scanning lidar, imaging spectrometer, and physically-based modeling for mapping snow water equivalent and snow albedo', *Remote Sensing of Environment*, 184, pp. 139–152. Available at: https://doi.org/10.1016/j.rse.2016.06.018.

Payne, J.T. *et al.* (2004) 'Mitigating the effects of climate change on the water resources of the Columbia River Basin', *Climatic Change*, 62(1–3), pp. 233–256. Available at: https://doi.org/10.1023/B:CLIM.0000013694.18154.d6.

https://doi.org/10.5194/essd-2026-303
Preprint. Discussion started: 30 June 2026

Pierce, D.W. *et al.* (2008) 'Attribution of declining Western U.S. Snowpack to human effects', *Journal of Climate*, 21(23), pp. 6425–6444. Available at: https://doi.org/10.1175/2008JCLI2405.1.

Plummer, D.A. *et al.* (2006) *Climate and Climate Change over North America as Simulated by the Canadian RCM*.

Pranab Kumar Sen (1968) 'Estimates of the regression coefficient based on Kendall's tau', *Journal of the American Statistical Association*, (63), pp. 1379–1389. Available at: https://doi.org/10.1080/01621459.1968.10480934 (Accessed: 11 March 2026).

Rahimi, S. *et al.* (2024) 'An overview of the Western United States Dynamically Downscaled Dataset (WUS-D3)', *Geoscientific Model Development*, 17(6), pp. 2265–2286. Available at: https://doi.org/10.5194/gmd-17-2265-2024.

Räisänen, J. (2008) 'Warmer climate: Less or more snow?', *Climate Dynamics*, 30(2–3), pp. 307–319. Available at: https://doi.org/10.1007/s00382-007-0289-y.

Roberts-Pierel, B.M., Raleigh, M.S. and Kennedy, R.E. (2024) 'Tracking the Evolution of Snow Drought in the U.S. Pacific Northwest at Variable Scales', *Water Resources Research*, 60(7). Available at: https://doi.org/10.1029/2023WR034588.

Rupa Rajulapati, C. *et al.* (no date) 'The Perils of Regridding: Examples Using a Global Precipitation Dataset'. Available at: https://doi.org/10.1175/JAMC-D-20.

Shi, H.X. and Wang, C.H. (2015) 'Projected 21st century changes in snow water equivalent over Northern Hemisphere landmasses from the CMIP5 model ensemble', *Cryosphere*, 9(5), pp. 1943–1953. Available at: https://doi.org/10.5194/tc-9-1943-2015.

Siegel, J.E., Fullerton, A.H. and Jordan, C.E. (2022) 'Accounting for snowpack and time-varying lags in statistical models of stream temperature', *Journal of Hydrology X*, 17. Available at: https://doi.org/10.1016/j.hydroa.2022.100136.

Solander, K.C., Bennett, K.E. and Middleton, R.S. (2017) 'Shifts in historical streamflow extremes in the Colorado River Basin', *Journal of Hydrology: Regional Studies*, 12, pp. 363–377. Available at: https://doi.org/10.1016/j.ejrh.2017.05.004.

Stewart, I.T., Cayan, D.R. and Dettinger, M.D. (2005) *Changes toward Earlier Streamflow Timing across Western North America*. Available at: http://tao.

Switanek, B.M. *et al.* (2017) 'Scaled distribution mapping: A bias correction method that preserves raw climate model projected changes', *Hydrology and Earth System Sciences*, 21(6), pp. 2649–2666. Available at: https://doi.org/10.5194/hess-21-2649-2017.

https://doi.org/10.5194/essd-2026-303
Preprint. Discussion started: 30 June 2026

Tabari, H. *et al.* (2021) 'Comparison of statistical downscaling methods for climate change impact analysis on precipitation-driven drought', *Hydrology and Earth System Sciences*, 25(6), pp. 3493–3517. Available at: https://doi.org/10.5194/hess-25-3493-2021.

Trujillo, E. and Molotch, N.P. (2014) 'Snowpack regimes of the Western United States', *Water Resources Research*, 50(7), pp. 5611–5623. Available at: https://doi.org/10.1002/2013WR014753.

Vandal, T. *et al.* (2017) 'DeepSD: Generating high resolution climate change projections through single image super-resolution', *Proceedings of the ACM SIGKDD International Conference on Knowledge Discovery and Data Mining*. Association for Computing Machinery, pp. 1663–1672. Available at: https://doi.org/10.1145/3097983.3098004.

Vernon, B., Zhang, W. and Chikamoto, Y. (2025) 'Improving seasonal precipitation forecasts in the Western United States through statistical downscaling', *Environmental Research Letters* , 20(6). Available at: https://doi.org/10.1088/1748-9326/add02c.

Vrac, M. *et al.* (2025) 'Should We Use Quantile-Mapping-Based Methods in a Climate Change Context? A "Perfect Model" Experiment', *Climate*, 13(7). Available at: https://doi.org/10.3390/cli13070137.

Walton, D.B. *et al.* (2017) 'Incorporating snow albedo feedback into downscaled temperature and snow cover projections for California's Sierra Nevada', *Journal of Climate*, 30(4), pp. 1417–1438. Available at: https://doi.org/10.1175/JCLI-D-16-0168.1.

Wood, A.W. *et al.* (2004) 'Hydrologic implications of dynamical and statistical approaches to downscaling climate model outputs', *Climatic Change*, 62(1–3), pp. 189–216. Available at: https://doi.org/10.1023/B:CLIM.0000013685.99609.9e.

Zakeri, F., Mariethoz, G. and Girotto, M. (2024) 'High-Resolution Snow Water Equivalent Estimation: A Data-Driven Method for Localized Downscaling of Climate Data'. Available at: https://doi.org/10.5194/egusphere-2024-1943.

Zarei, E. *et al.* (2025) 'Hybrid deep learning downscaling of GCMs for climate impact assessment and future projections in Oman', *Journal of Environmental Management*, 376. Available at: https://doi.org/10.1016/j.jenvman.2025.124522.

Zeng, X., Broxton, P. and Dawson, N. (2018) 'Snowpack Change From 1982 to 2016 Over Conterminous United States', *Geophysical Research Letters*, 45(23), pp. 12,940-12,947. Available at: https://doi.org/10.1029/2018GL079621.

(No date) 'Daymet: Daily Surface Weather Data on a 1-km Grid for North America, Version 4 R1 Get Data'. Available at: https://doi.org/10.3334/ORNLDAAC/2129.